UNIVERSITÀ DEGLI STUDI DI PADOVA

DIPARTIMENTO DI INGEGNERIA INDUSTRIALE

CORSO DI LAUREA MAGISTRALE IN INGEGNERIA DEI MATERIALI

MSc work carried out at the Chair of Nonferrous Metallurgy - Montaniniversität Leoben

Fast Scanning Calorimetry on Al-Mg intermetallic phases

Relatori: Prof.ssa Irene Calliari

Prof. Dipl.-Ing. Dr.mont. Stefan Pogatscher

Laureando: Alberto Mezzacasa

Matricola: 1154352

ANNO ACCADEMICO 2017-2018

Alla mia numerosa e meravigliosa famiglia.

Abstract

This thesis aims to analyse the intermetallic compound Al_3Mg_2 using Fast Differential Scanning Calorimetry (FDSC). This compound has been selected because its unit cell is complex and, to be precise, it is composed by 1168 atoms. It is assumed that it is therefore possible to induce the formation of metastable or glass phases thanks to the high cooling rates that the FDSC allows to reach. In addition, it is to be verified if the application of high heating rates leads to the formation of a liquid intermediate during the solid-solid transition, as already seen in a study on another metallic alloy.

The work is made up of two parts: in the first part there is a detailed description of the preparation of the samples, which has required a great deal of effort due to the several difficulties encountered. The procedure starts with high purity raw materials which are placed inside a quartz tube. An inert atmosphere is created inside the tube and vacuum is applied. The use of a Graphite crucible helps to prevent the formation of impurities in the intermetallic compound. The material is melted using an inductor. The composition of the material is analysed using Optical Microscope (OM), Scanning Electron Microscope (SEM) and Differential Scanning Calorimetry (DSC).

Once the quality of the intermetallic compound has been verified, in the second part of this work, different temperature programs are applied using the Flash DSC 1. This instrument allows to analyse small samples with very high cooling or heating rates. There is a focus on the identified solid-solid phase transition, that is not foreseen by the phase diagram. In addition to various analyses on this event, which is an exothermic phase transition, the change of the melting temperature due to the change in the applied heating rate to the sample is also analysed.

The experimental work was performed in Leoben (AT), at Montanuniversität Leoben - Chair of Nonferrous Metallurgy, under the supervision of Prof. Dipl.-Ing. Dr.mont. Stefan Pogatscher.

Riassunto

Questo lavoro di tesi ha l'obiettivo di analizzare il composto intermetallico Al_3Mg_2 facendo uso della Fast Differential Scanning Calorimetry. Tale composto è stato selezionato in quanto la sua cella unitaria è complessa ed è composta da 1168 atomi; si presuppone che sia dunque possibile indurre la formazione di fasi metastabili o vetrose grazie alle elevate velocità di raffreddamento che la FDSC permette di raggiungere. Inoltre, si vuole verificare se l'applicazione di elevate velocità di riscaldamento portano alla formazione di un intermedio liquido durante la transizione solido-solido, come già visto in uno studio su un'altra lega metallica.

Il lavoro è composto da due parti: nella prima parte c'è un'approfondita descrizione della preparazione dei campioni che ha richiesto molto impegno a causa delle numerose difficoltà incontrate. La procedura ha inizio da materie prime ad alta purezza le quali vengono poste all'interno di un tubo di quarzo. All'interno del tubo viene creata un'atmosfera inerte e viene applicato il vuoto. L'uso di un crogiolo di grafite permette di prevenire la formazione di impurità nel composto intermetallico. Il materiale viene fuso per mezzo di un induttore. Il materiale viene analizzato per valutare la composizione usando il microscopio ottico, il microscopio elettronico a scansione (tecnica EDS) e la calorimetria a scansione differenziale (DSC).

Verificata la qualità del composto intermetallico si procede, nella seconda parte della tesi, all'applicazione di diversi programmi di temperatura usando la Flash DSC 1. Questo strumento permette di analizzare campioni di piccole dimensioni con elevatissime velocità di raffreddamento o riscaldamento. Si studia in particolare la transizione di fase solido-solido individuata e non prevista dal diagramma di stato. Oltre a varie analisi su questo evento che è di natura esotermica, si analizza anche la variazione della temperatura di fusione dovuta alla variazione della velocità di riscaldamento del campione.

La parte sperimentale di questo lavoro è stata svolta a Leoben (AT), presso la Montanuniversität Leoben - Chair of Nonferrous Metallurgy, sotto la supervisione del Prof. Dipl.-Ing. Dr.mont. Stefan Pogatscher.

Contents

1 Introduction

The first chapter describes briefly the results previously obtained by using DSC Flash. Below there is an in-depth description of the intermetallic compound with some historical notes about its study: identification, crystallographic analysis and polymorphism analysis. Finally, a short description of the evolution of the thermal analysis techniques that led to the development of Fast Scanning Calorimetry is given.

1.1 Solid-solid phase transitions via melting

A recent study has presented experimental evidence for a solid–solid transition via the formation of a metastable liquid in a 'real' atomic system [1]. This observation represents a novelty in the field of physical metallurgy and it was only possible thanks to the use of Fast Differential Scanning Calorimetry. This technique, that will be described in depth later, has a sufficient temporal and spatial resolution to be able to detect small and fast phase transitions at high heating or cooling rates.

The results have been obtained on small-scale $Au_{70}Cu_{5.5}Ag_{7.5}Si_{17}$ specimens which have been amorphized *in-situ* via rapid cooling at a rate of 5000 K/s. Different heating rates have been applied (Figure 1-1 a). An increase of the heating rate causes the shifts of the crystallization temperature onset T_1 end T_2 to higher temperatures, which is normally expected for the crystallization of supercooled liquids and most solid–solid transitions [2]. A surprising endothermic effect was detected at T_e (≈558 K) after the T_1 peak and right before the T_2 peak for heating rates higher than 350 K/s. The endothermic effect does not show rate dependence; this means that it corresponds to a melting event [1].

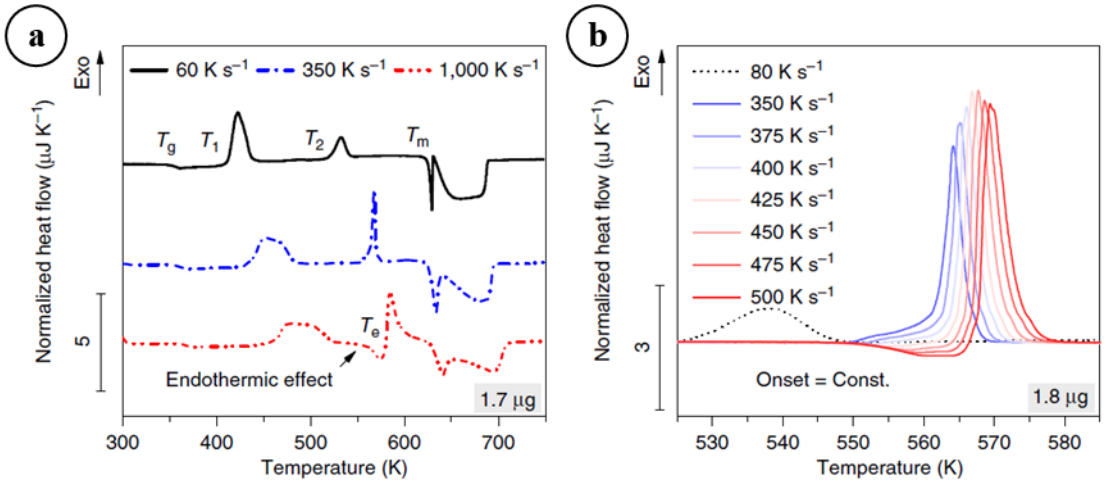

Figure 1-1 a) *FDSC heat flow curves normalized to the heating rate;* ***b)*** *Detail of the start of the endothermic effect and the second exothermic peak (T_2) [1].*

So, the solid-solid transition from the metastable phase to the stable phase passes through the formation of a metastable liquid (Figure 1-2). The bulk metallic glass exhibits the following unusual transition path upon heating [1]:

glass
↓
undercooled liquid
↓
metastable crystalline state
↓
metastable liquid
↓
'stable' crystalline state
↓
equilibrium liquid

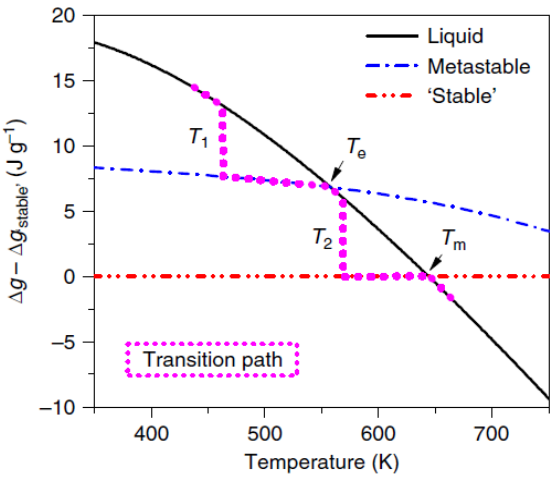

Figure 1-2 *Gibbs free energy diagram. The magenta dotted line represents the transition path upon heating [1].*

It is supposed that this concept could be applied to any metastable to more stable transformation of crystals and does not require the glassy state. From this consideration arise the idea to analyse an intermetallic compound in the Aluminium–Magnesium (Al-Mg) system.

Because of its high complexity, β-Al_3Mg_2 could be an excellent candidate for the study of solid-solid phase transition because the amorphization or the formation of a metastable phase would be more probable. It is expected to be able to obtain a metastable phase after a rapid quenching from the melt using the Flash DSC 1 (Mettler Toledo).

When a material is quenched from the molten state it is possible to induce the formation of metastable solid states not predicted by equilibrium phase diagrams: solid phases with higher solute concentration, new metastable crystalline phases or amorphous metallic glasses [2].

1.2 Al_3Mg_2 phase

Because of their low mass density, Al-Mg alloys are widely used in technological applications. For this reason, the phase diagram (Figure 1-3) has been studied several times not always leading to an improvement on the previous ones.

In the Al–Mg system a few rather complex intermetallic compounds are present. Intermetallic compounds, unlike solid solutions, are characterized by a restricted composition of existence and usually have stochiometric composition [2]. β-Al_3Mg_2 (cF1168) is the one with the highest complexity [3] in this system.

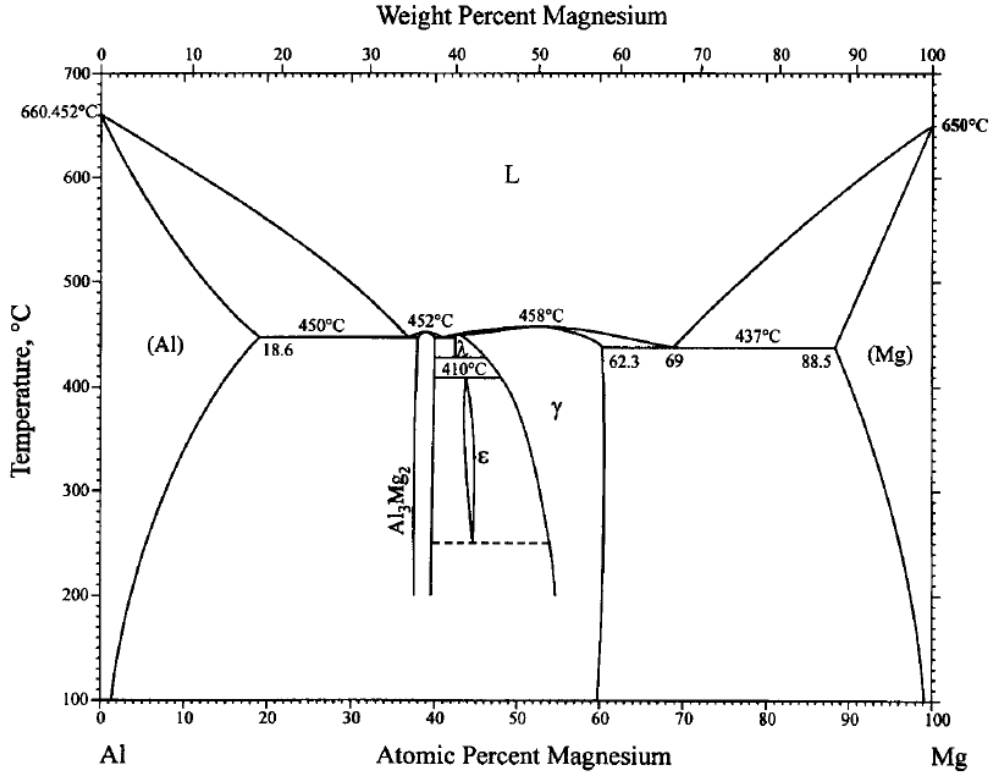

Figure 1-3 *Al-Mg phase diagram [4].*

Riederer (1936) established the existence of the β phase in the Aluminium-Magnesium system. He proposed, on the basis of powder diffraction studies, eight formula units of

Al_8Mg_5 per unit cell and a hexagonal structure with cell parameters a = 11.40 Å and c = 17.99 Å; the measured density was ρ = 2.23 g/cm^3. Laves and Möller (1938) were able to determine, from powder patterns observation, that the β phase is isomorphous with Cu_4Cd_3. Afterwards, Perlitz (1944, 1946) analysed a small fragment of an alloy which composition was 38% Mg and 62% Al by weight; he determined that it represents a cubic structure, space group $Fd\bar{3}m$ (O_h^7, Schoenflies notation), with approximately 1166 atoms per unit cube of edge a_0 = 28.22 Å. He used the density previously given by Riederer to determine the unit-cell content; then he assumed the composition Al_3Mg_2 [5].
Samson (1965) prepared Aluminium-Magnesium alloys of various composition and was able to obtain three single-phase samples with the compositions shown in Table 1-1.

Table 1-1 *Single phase β-Al_3Mg_2 sample used by Samson (1965) [5].*

Mg [wt.%]	Al [wt.%]	Formula	Density ρ [g/cm^3]
37.83	62.10	$Al_{2.96}Mg_2$	2.249
37.47	62.49	$Al_{3.01}Mg_2$	2.224
36.23	63.76	$Al_{3.17}Mg_2$	2.229

This intermetallic phase is characterized by very low density.
Chemical analyses and measures of densities have been performed on the three samples mentioned above and these gave the following number of atoms in the unit-cell for a_0 = 28.239 Å:

Table 1-2 *Atoms per unit cube in Al_3Mg_2 samples with different composition [5].*

Phase composition	Number of atoms in the unit-cell
$Al_{703}\,Mg_{475}$	1178
$Al_{699}\,Mg_{465}$	1164
$Al_{714}\,Mg_{451}$	1165

The composition range of existence for the β phase is slightly variable. In particular the β phase exist in the range 37.5 - 40 at.% of Mg [4].

More recently, the Al-Mg phase diagram has been reinvestigated in the proximity of the stability range by Steurer [3]. For the composition $Al_{61.5}Mg_{38.5}$, this cubic phase presents a space group $Fd\bar{3}m$ (n° 227) with a = 28.242 Å, V = 22526 Å^3. At 214 °C undergoes a first-order phase transition to rhombohedral β'-Al_3Mg_2 (hR293) which parameters are a = 19.968 Å, c = 48.9114 Å and V = 16889 Å^3 (i.e. 22519 Å^3 for the equivalent cubic unit cell). The space group is R3*m* (n° 160), a subgroup of index four of $Fd\bar{3}m$.
The structure of β'-Al_3Mg_2 is strictly related to the structure of the β phase. The position of its atomic sites can be obtained by group-theoretical considerations from those of the β phase. The main difference between the two structures is that while in the β phase there are empty atomic sites, in the case the β' phase they are fully occupied [3].

1.2.1 Al_3Mg_2 Structure

The β-Al_3Mg_2, also called Samson phase, is a polytetrahedral intermetallic compound composed by 672 icosahedral clusters, 252 truncated tetrahedra (also called Friauf polyhedra) and 244 more-or-less irregular polyhedra of ligancy 10 to 16, of which 48 are modified Friauf polyhedra. "It shows many partially occupied and split positions leading to only 1168 atoms per unit cell instead of the 1832 ones expected from the multiplicity of the partially occupied Wyckoff positions" [3]. About 75% of atoms (879 to be exact) form the skeleton of the structure; 528 of them are Al and 351 are Mg. By "the framework" or "skeleton atoms" it is possible to identify a set of atoms positions which are occupied with the probability of 100%. The other 289 (25%) atoms does not occupy a specific position; there is an average occupation probability of 30% in the partially occupied 953 positions

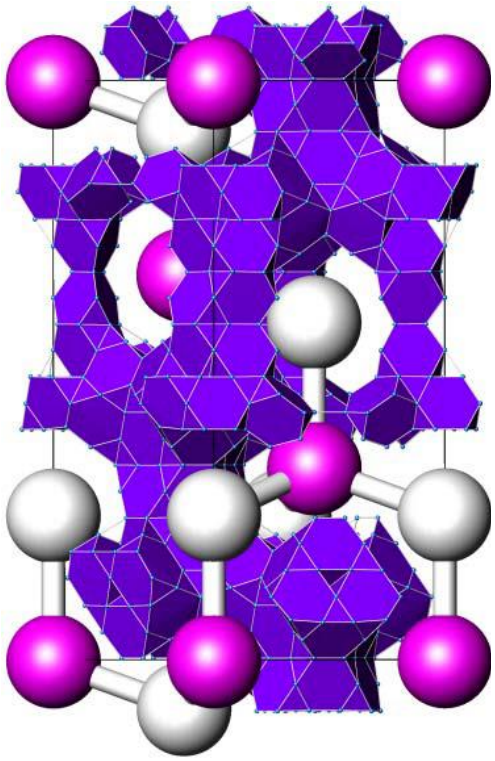

Figure 1-4 *Clusters making up a diamond network with Friauf polyhedra in-between [3].*

available [6]. These atomic sites could be partially occupied (structural vacancies) or split positions (structural half vacancies) [3].

"The clusters are packed in a diamond network, and in-between the clusters there is a framework of face sharing Friauf polyhedra" [3], as illustrated in Figure 1-4.

The skeleton atoms of a Samson phase are arranged in hexagonal layers. These layers form three structural domains, which are shifted each other by 1/3 of the length of the main diagonal of the cubic unit structure. The whole structure is composed by 22 parallel and equally distant layers. Some of them are occupied by the skeleton atoms, the rest is filled by atoms forming clusters [7].

1.2.2 Polymorphism β → β'

At the temperature of 214 °C a phase transformation from the cubic to the rhombohedral structure occurs. "It should be pointed out that the constant c of the rhombohedral structure is practically equal to the length of the diagonal of the cubic structure $a_{cubic}\sqrt{3}$ = 4.89166 nm ≅ c_{rhomb}. The near equivalence in length between the c axis of the rhombohedral β'-Al_3Mg_2 structure and the diagonal of the cubic β-Al_3Mg_2 is a consequence of lattice transformation connecting the hR cell of the β' phase to the F cell of the β phase. During that transformation, positions of the skeleton atoms do not change" [7].

The transformation from the high temperature β phase to the low temperature β' phase leads the break of clusters into short chains hexagonal layers of different size and results in reducing the symmetry of a single domain; one symmetrical domain becomes asymmetric. This process undergoes at different temperatures with the size of the chain. Instead of classical phase transition this one is characterized by a diffuse-controlled behaviour, which also depends on the annealing time of the sample [6].

β'-Al_3Mg_2 is the stable phase at low temperature but it needs a long time to form. That means that after the cooling it is possible to obtain a metastable β-Al_3Mg_2 at room temperature. In his study Steurer [3] were able to trace β'↔β transformation by differential scanning calorimetry on a sample that was annealed at 170 °C for 42 days.

They demonstrated with X-Ray powder diffraction analysis that the high-temperature β-Al_3Mg_2 is kinetically stabilized at temperature below 100 °C and that its lattice parameter is linearly dependent on the temperature; whereas at temperature between 100 and 200 °C the phase transition β↔β' could be obtained [3].

1.3 Chip calorimetry

From the second half of the twentieth century the demand for thermal analysis and calorimetry equipment begin to grow. This happened because these analytical techniques are crucial for the study of thermal proprieties of substances and materials. Over the decades many improvements have been done to these devices to improve the quality of the analysis and to allow higher scanning rates.

New capability arose by the introduction twin calorimeters. These consist of two cells, one with a sample and one empty as reference, which allow to measure the differences between the two thermal response of the sample to the applied temperature program. The newly developed twin calorimeters are characterized by smaller furnaces and cells; this make possible to use samples with smaller mass, in the range 1-100 mg. The resulting Differential Scanning Calorimeters (DSCs) can run temperature-time program at constant scan rates, about 10 K/min, for both cooling and heating ramps.

Further developments allowed to reach higher rates, up to 2000 K/min (Rapid Heating and Cooling DSC). For such high rates, in order to achieve high scan rate, it is necessary to reduce as much as possible the dimension of the sample; in this way the thermal lag is reduced.

The reason of such interest into increase the cooling and heating rates is the attention on fundamental studies of the crystallization, phase transitions and melting behaviour of materials. Furthermore, it is of great interest to study amorphization and partial to full crystallization of materials at high rates. High rates could in fact reproduce what happen during industrial processes and be fast enough to prevent, fully or partially, reorganization phenomena.

The ability to reach these high rates became real with the introduction of chip-based calorimeters. The first instrument to be commercially available was Flash DSC 1 (Mettler Toledo). This new instrument has aroused great interest because it allows a wide range of heating and cooling rates to be investigated: from 0.1 to 40,000 K/s.

Nowadays it is widely used for the study of amorphization and solid-solid or solid-liquid transitions both on polymeric [8,9] or metallic materials [10]. Furthermore there is a lot of interest in this technology also in other fields as pharmaceutical (to study metastable phases behaviour or degradation phenomena [11]) and food.

The reason that arouse more interest is the possibility to analyse non-equilibrium transformations. For example, Kurtuldu, Shamlaye et al. (2018) [12] has recently published

a study about metastable quasicrystal-induced nucleation. This kind of analysis, and many more, were not possible before chip calorimetry.

The expectation from this study is to exploit the potential of Flash DSC 1 to explore the phase transition of the β-Al_3Mg_2 in non-equilibrium conditions.

2 Characterization methods

The second chapter describes the different characterisation techniques used. More importance is given to the description of the DSC and FDSC thermal analysis techniques because they are the main focus of the study and because the FDSC is the result of the development of the previous one. Finally, also the microscopy techniques used to characterize the composition of the intermetallic compound are discussed

2.1 Thermal analysis techniques

Thermal analysis is a group of techniques in which one or more properties and characteristics of a sample are studied. Nowadays there are a lot of different thermal analyses that allow the examination of a wide range of properties like mass, volume and dimensional changes, thermal diffusivity and conductivity, ΔT, heat flux and gas produced by decomposition [13]. The choice of the appropriate thermal analysis and temperature program depends on the properties that are of interest for the analysis

For the analysis of phase transformations there are two traditional techniques, very similar to each other but with different output:

- Differential Thermal Analysis (DTA): the signal is the temperature difference between sample and reference, typically plotted versus temperature (T).

  If e.g. a phase transformation occurs, the DTA signal makes a peak to the endothermic direction because the sample is colder than reference. The "onset" of this peak is the transformation temperature;
- Differential Scanning Calorimetry (DSC): due to a more sophisticated construction not only T itself, but additionally the heat flow into (or from) the sample can be measured. This allows, in addition to T, also to measure the heat energy (e.g. heat of melting) that is absorbed or released by the sample. If performed very carefully, also the measurement of specific heat capacity is possible [14].

In order to obtain a more detailed analysis of the intermetallic compound, during this study the DSC analysis is used.

2.1.1 Differential Scanning Calorimetry (DSC)

As is known from thermodynamics, every chemical reaction and many phase transitions are associate with the generation or consumption of heat; the main technique used for the analysis of phase transition and characteristic temperatures of reaction in materials science is the Differential Scanning Calorimetry (DSC). The DSC analysis could be accurately defined as:

"Differential Scanning Calorimetry (DSC) means the measurement of the change of the difference in the heat flow rate to the sample and to a reference sample while they are subjected to a controlled temperature program". [15]

It is easy to understand from the definition that the analysis is carried out using two crucibles. One is for the material that one wants to analyse while the other is for a reference; depending on the kind of analysis is performed the reference crucible could be left blank or not. Both the sample and the reference crucibles are subjected to the same time-temperature program because they are positioned inside the same furnace; a simplified scheme of the system is shown in Figure 2-1. In this way, if a change in a property occurs, it is possible to measure a difference in temperature between the two crucibles that could be transformed into a heat flow rate.

During this project a Netzsch DSC204 F1 Phönix was used. This instrument is equipped with a silver furnace with embedded heating coil. The high thermal diffusivity of the silver provides an excellent heat distribution inside the cell. This is very important for devices that work according to the heat flow principle. A sensor is installed right below the two crucibles; the difference in temperature between the crucibles is given as a voltage in the original signal and then automatically transformed as flow heat rate (dΔq/dt) by the instrument software [14].

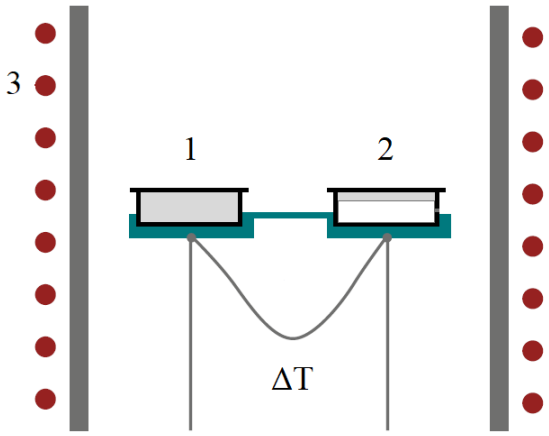

***Figure 2-1** Scheme of a heat flow DSC cell. **1**) sample; **2**) sample; **3**) silver furnace.*

The time-temperature program applied is a fundamental part of the test and should be customized for different samples; this allow to analyse different properties for different

materials. The program is usually composed by many segments; in the simplest cases it is just constituted by constant heating/cooling rate (dT/dt ≠ 0 = constant) and isothermal (dT/dt = 0) segments. In Figure 2-2 a standard DSC program for the analysis of melting is shown. It is possible to see that when the material reaches the melting temperature (T_m), during the heating, the temperature of the sample (T_s) remains constant until all the material is melted; on the other hand, in the reference crucible nothing happens, so the temperature of the reference (T_r) continues to rise linearly. This causes a changing in the difference of temperature between the two crucibles and thus a flow heat rate ($d\Delta q/dt \neq 0$) is detected. The result signal is shown in the lower part of the diagram; the endothermic peak corresponds to the melting event. In accordance with ICTAC rules, $T_s - T_r$ is positive for exothermic processes (exo) and negative for endothermic (endo) processes [16]. During the cooling the crystallization occurs at $T < T_m$ because of the effect of supercooling; this affect also the shape of the peak.

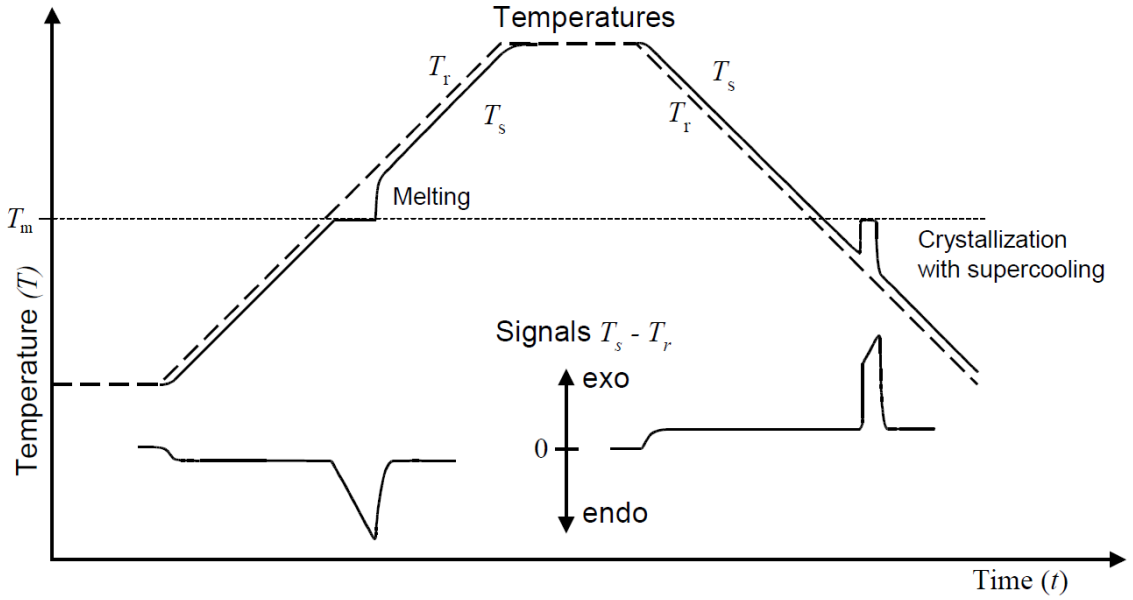

Figure 2-2 *The upper diagram shows the course of the temperatures of sample (T_s) and reference (T_r); the lower diagrams show the resulting signal $T_s - T_r$ [16].*

The heating and cooling rates for Netzsch DSC204 F1 Phönix are in the range 0.001 to 200 K/min and the maximum cooling rate achievable depends on which cooling option is used; the available options are compressed air, intracooler and liquid nitrogen.

Different kind of crucibles (or pans) can be used. It is necessary to avoid chemical interaction with the sample and to assure its resistance in the test conditions. They may be made of metal, graphite, glass or oxide ceramic.

The atmosphere in the cell may be oxidizing or inert and can be switched from one gas to another during the experiment [14]. In any case the presence of a protective gas does not guarantee absolute protection against oxidation phenomena at high temperatures.
The instrument set-up is shown in Figure 2-3.

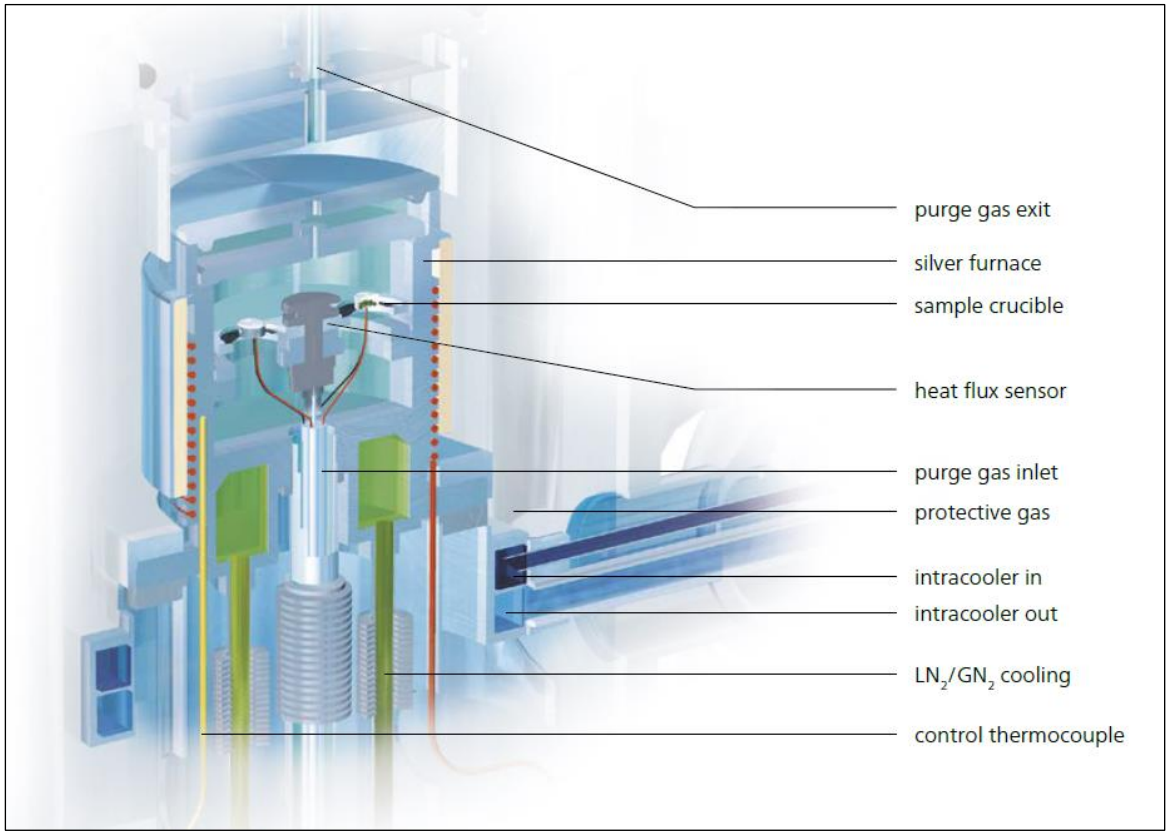

Figure 2-3 *Set-up of the Netzsch DSC 204 F1 Phoenix®.*

From the output curves of DSC analysis, it is possible to obtain many information. It is necessary to focus on the discontinuity points of the curve. These make it possible to identify glass transition temperature (T_g), onset and endset temperature (T_{onset}, T_{endset}) for solid-solid or solid-liquid transitions; furthermore, the shape of the discontinuity allows to obtain information about the kinetics of the transition.
As the height of a peak is proportional to the heat absorbed (or released) by the sample, if the pressure is kept constant, it is possible to determine the change in enthalpy (ΔH) do to phase transition (expressed in Joule). To do this it is necessary to make the integral of the peak between the measured T_{onset} and T_{endset}. An overlap of the peaks can make the analysis of the curve difficult [13].

It is possible to represent with a simple diagram the operation of a general DSC instrument (Figure 2-4).

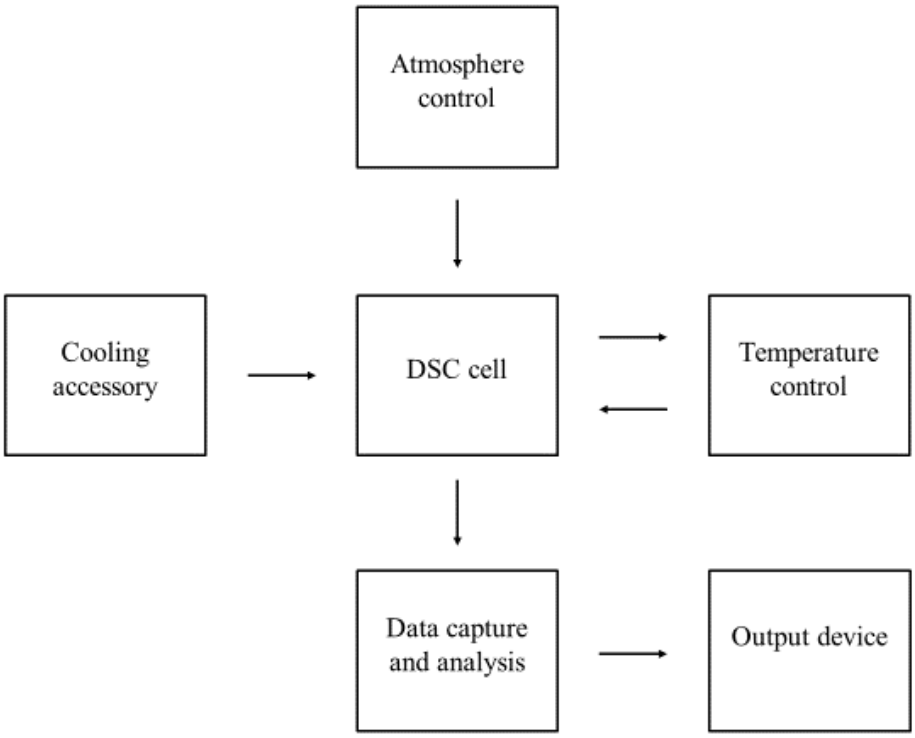

Figure 2-4 *Schematic representation of a DSC instrument [14].*

2.1.2 Fast Differential Scanning Calorimetry

The need to achieve very fast cooling rates has led to the development of fast scanning calorimetry or chip calorimetry. This technology can reach such high cooling and heating rates that allows the analysis of reorganizational phenomena and the kinetics of fast transformations.

In this study the purpose is to analyse the phase transitions of the intermetallic compound β-Al_3Mg_2 in order to see if it is possible to obtain metastable phases during cooling and if during the subsequent heating the metastable-stable transition via-liquid is proposed again as in the study mentioned above. It is necessary to use this instrument instead of a conventional DSC because the reorganizational phenomena in metals are very fast.

This intermetallic compound was chosen because of its complexity and because its melting temperature falls within the temperature range in which the instrument, the Flash DSC 1 Mettler Toledo, can be used. A detailed description of the instrument is given in §2.1.2.2 .

2.1.2.1 The Calorimeter

A simple model, from *Fast Scanning Calorimetry [15]*, can be used to represent and discuss many aspects of fast scan calorimetry.

It is possible to consider a calorimeter with the heat capacity C_c and at temperature T_c. The calorimeter is surrounded by a gas that is at temperature T_{gas}.

The temperature of the calorimeter could be changed by a heater, which is powered by electricity. The power given to the system is represented in Figure 2-5 by P_{el}. The temperature T_{gas} is lower than T_c and for this reason there is a loss of energy from the calorimeter to the surrounding (P_{loss}).

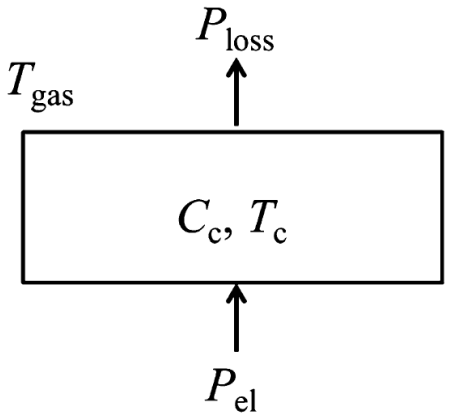

Figure 2-5 *Simplified model of a calorimeter [17].*

$$P_{loss} = -\frac{\Delta T}{R_{GC}} \qquad (2\text{-}1)$$

P_{loss} is influenced by the difference in temperature between the calorimeter and the surrounding (T_c-T_{gas}) and by the thermal resistance (R_{GC}) between the calorimeter and the surrounding gas. This thermal resistance depends on the type of gas, the pressure, and the size of the calorimeter.

$$P_{el} = -\frac{\Delta T}{R_{GC}} = C_C \cdot \beta \qquad (2\text{-}2)$$

Where $\beta = (dT_c/dt)$ is the scanning rate.

After this short description of the model of the calorimeter it is possible to say that:

- the calorimeter must have a small heat capacity to reach high heating rates. This is possible as much as the volume of the calorimeter is small;
- the surrounding gas should be at the lowest possible temperature to increase the maximum cooling rate achievable. It is also possible to achieve high speeds by increasing the heat conductivity of the gas.

The calorimeter of Flash DSC 1 is made of a thin Si_3N_x-membrane with the electronic components for the heater and temperature sensor.

2.1.2.2 The Flash DSC 1

The Flash DSC 1 (Figure 2-6) is a commercial instrument that can achieve really high heating and cooling rates; using a MultiSTAR USF1 sensor, that has a time constant smaller than 1 ms, it is possible to run experiments using rates that extend from 0.5 to 40,000 K/s (30 - 2,400,000 K/min). The achievement of all the range of rates is influenced by experimental conditions, the temperature range and the proprieties of the sample.

Figure 2-6 *The Flash DSC 1 Mettler Toledo.*

Thermal analysis programs for the Flash DSC 1 are implemented by STARe Software that is directly provided by Mettler Toledo. This software allows to create personalized programs containing up to 200 segments (heating, cooling or isothermal segments). Furthermore, it is possible to do a lot of different evaluations and corrections on the output curves (measurements of onset and endset temperature, integrations, temperature corrections with references). The instrument is equipped with an optical microscope to facilitate the user during the positioning of samples; in fact, the samples are smaller than 200 μm and it is necessary to pick them up using the bristle of a brush. An IntraCooler is provided with the instrument and it allows to reach a temperature about -100 °C in the surrounding of the sample; during this specific study the minimum temperature reached in the experiments is -90 °C. Argon is used as purging gas; its function is to cool the sensor support and also to prevent oxidation at high temperature.

The sensor is constituted by a ceramic frame; in the middle of the ceramic frame there is the DSC sensor. The specified maximum temperature of use is 450 °C; if it is possible to accept a higher noise and a reduced life time it is possible to reach about 520 °C.
The contact between the sensor and the instrument is made through pins (Figure 2-7).
A good electrical contact is favourited by a clamping disk that fix the position of the sensor on the instrument.
On the chip sensor there are eight thermocouples that allow to measure the temperature of sample and reference. It is necessary to use the temperature of the sensor support (T_{ss}) as a reference temperature for the cold junction. T_{ss} is also the temperature of the surrounding gas; in practice it is always necessary to wait a certain time to reach the equilibrium between the gas temperature and the temperature of the sensor support.

Figure 2-7 *The UFS 1 chip sensor and the sensor support with electrical contact pins [13].*

The T_{ss} can be set in three different states depending on the situation: "ready", "standby temperature" and "power off". Using STARe it is possible to define from the module window the ready and standby temperature; usually the standby temperature is in the range between 10 and 40 °C. In the "power off" setting the temperature is not controlled. It is used when there are long brakes between successive measurements.
The correction procedure can be performed on the sensor when T_{ss} is equal to the ready temperature; it is necessary to adjust the thermocouple on the sensor with respect to T_{ss}.

2.1.2.3 Sensor design

Here is a short description of the chip sensor MultiSTAR UFS1 provided by Mettler Toledo and used for β-Al_3Mg_2 analysis. The sensor, that is embedded in a ceramic support, is based on MEMS technology (Micro-Electro-Mechanical System). There are two different calorimeters: one for the sample and one for the reference (see Figure 2-8). The two calorimeters operate like a conventional DSC, but in this case, there is not a real crucible; the sample is just positioned on the calorimeter to run the experiments.

The twin calorimeters are made by two layers: the first one is made of Silicon nitride membrane while the second one is made of Silicon oxide. The total thickness of the membrane is 2 μm. The length of each quadratic membranes is 1.6 mm. They are mounted on a silicon frame, which thickness is 300 μm. The central zone of the membrane is coated with aluminium; this works as heater and allows to achieve a more homogeneous temperature profile on the calorimeter and then on the sample.

In Figure 2-9 is possible to see how every single chip could be identified thanks to a serial number; the number it very important because it is necessary for the correction procedure. Also the contact pins are visible; half of them are necessary for the heating, the other half is due to temperature measurements.

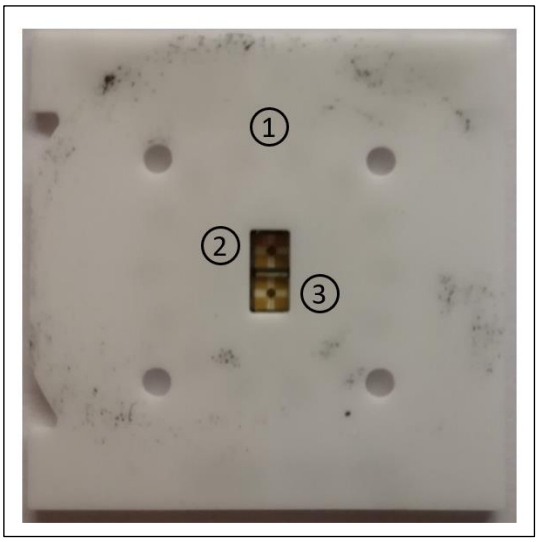

Figure 2-8 *Chip sensor - TOP.*

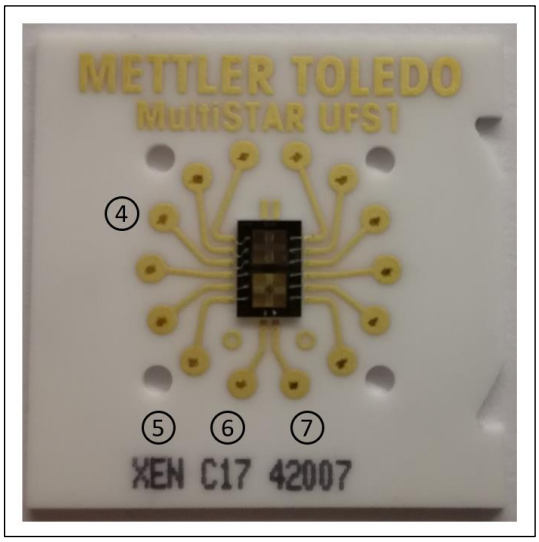

Figure 2-9 *Chip sensor – BOTTOM.*

Table 2-1 *Description of references in Figure 2-8 and Figure 2-9.*

.Reference	Description	Reference	Description
1	Substrate (ceramic plate)	4	Contact pins
2	Sample side	5	Type
3	Reference side	6	Year of manufacturing
		7	Serial number (continuous)

A more detailed and schematic representation of the chip sensor is given in Figure 2-10.

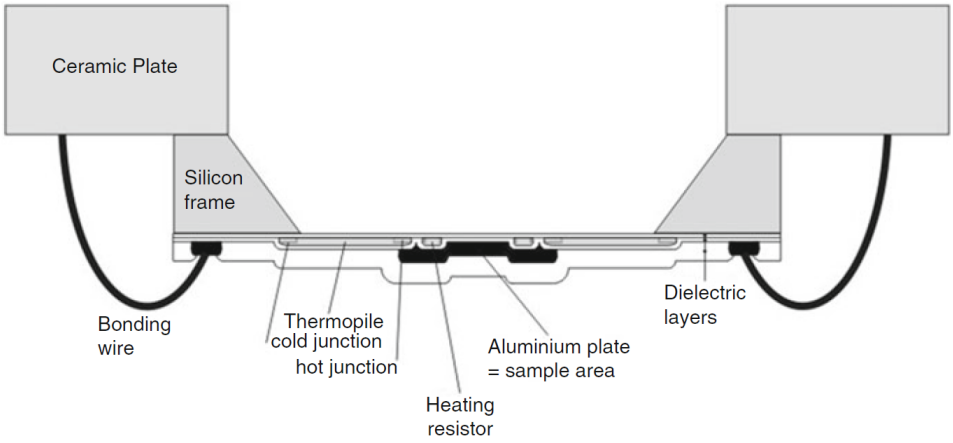

Figure 2-10 *Schematic representation of the UFS1 Sensor [17].*

It is possible to see the position of the different layers, the Aluminium coated area and the position of the resistor for the heating. The electrical connection between the Silicon frame and the ceramic plate is made by bonding wires.
The volume of the furnace is approximately $4x10^{-13}$ m^3; the density is circa 3.2 g/cm^3 and the specific heat capacity 0.5 J/g·K. This means that the heat capacity of the furnace is circa 600 nJ/K. For this reason, the maximum cooling rate achievable is around 10,000 K/s.

2.1.2.4 Operation mode of the Flash DSC 1

As already described for the conventional DSC, also del Flash DSC 1 operates in a power compensated mode. So, the difference in temperature between the furnaces is kept to zero modulating the amount of power. The micro-fabrication process used to produce the chip guarantees an excellent symmetry between the calorimeters. This can be easily verified with simple experiments using Indium [17].

2.1.2.5 Placing the sensor

The installation of the sensor is a very important procedure; if it is not properly done there could be a certain inaccuracy in the measurements. So, it is better to follow several steps as recommended in *"Fast Scanning Calorimetry"* [17]:

- From the STARe installation window select the "ready" or "standby temperature". The "ready" temperature should be selected only if the device is ready for the measurement; so, just if the ready temperature is the same as the support temperature (T_{ss}). The lower is the ready temperature, the higher could be the cooling rate achievable. But the lower is the temperature, the higher is the time necessary to stabilize the temperature before the measurements;
- The sensor must be identified using the serial number and then clamped on the sensor support. Afterwards it is possible to run the conditioning procedure. This program should be run twice (during this study it has be done four times). It reaches the maximum temperature possible for the chip; it is necessary to delete potential memory effect or stress in the membrane. For the UFS1 chip sensor the maximum temperature is 520 °C but it is advise against to use a temperature higher than 450 °C for the experiment because this reduces the time life of the sensor;
- The lid of the instrument should be closed when the correction procedure is performed. It is also necessary to wait for the equilibrium between the ready temperature and T_{ss}; otherwise, the accuracy of the measurements will not be good. This procedure is performed to correct the signal of the thermocouple with respect to the cold junction temperature (T_{ss}). The T_{ss} used is -90°C;
- When the correction procedure is finished, it is possible to set the standby temperature and then open the lid;
- When the lid is open the sample could be placed on the sensor. At first it is better to melt the sample; in this way the area of contact between the sample and the sensor increase;
- The lid can be closed and the temperature can be set on ready temperature; when the ready temperature is equal to T_{ss} it is possible to start the measurements.

2.1.2.6 Sample preparation for FDSC

As already written above, the sample is placed directly on the furnace area in the middle of the sensor. During the first tests on the intermetallic compound, it was not possible to melt the samples; so, tests are performed using samples scratched from the surface of a polished piece of material. This ensured at least one flat surface in the sample and so a better contact with the furnace surface (see Figure 2-11 a).

All the tested samples are obtained using a specific knife or scalpel. The blade is part of a series of tools given with the device. Using the knife it is possible to scratch the surface of the material and obtain a lot of small samples. In these experiments just samples in the dimensional range from 50 to 200 μm (for the bigger dimension) are used. The reason of this range in the size is due to:

- The diameter of the round furnace is about 500 μm; the sample must fit inside this area in order to be heated homogeneously;
- The larger the sample size, the more difficult it is to cool it with high cooling rate (e.g. 10,000 K/s) without thermal lag in the signal;
- The smaller the sample size, the weaker the signal given by the instrument. So, eventually, low enthalpy reaction cannot be detected.

The samples are previously analysed and measured with the optical microscope installed on the Flash DSC 1 and then placed on the chip sensor.

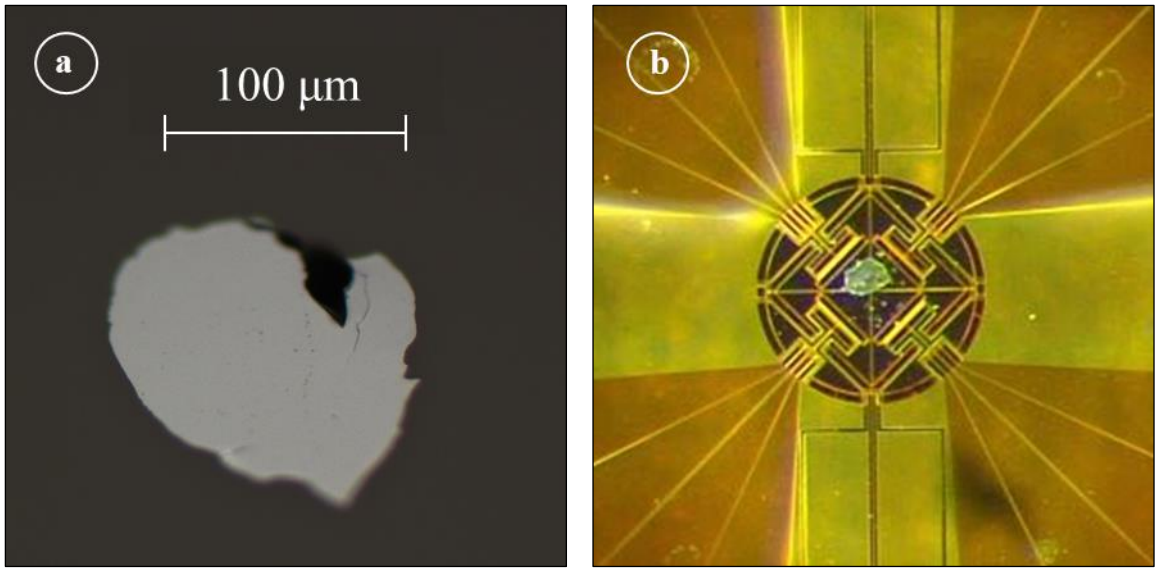

***Figure 2-11 a**)Example of a sample measured with the optical microscope and used in the Flash DSC 1;* ***b**) Example of a sample positioned on the chip sensor.*

The sample can be positioned using the bristle of a brush or a hair with a naturally grown tip. Sometimes the procedure could be difficult due to electrostatic phenomena. These kinds of problems could be avoid taking some precautions that are listed in *"Fast Scanning Calorimetry"* [17].

2.2 Light Optical Microscopy

Light optical microscopy is a common first step for analysis of metallic materials. It allows the analysis of microstructural characteristics such as: shape and size of grains, presence of different phases, inclusions and defects.

Optical microscope (OM) uses visible light and a system of lenses to magnify images of small subjects. Because of it uses visible light the maximum resolution is about ~1 μm. Furthermore, the depth of field is low, so it is necessary to have flat specimens.

The analyses of the intermetallic compound are done using a Zeiss Axio Imager M1 (Figure 2-12). This device is equipped with 7 objectives with magnification from 2.5 to 200X. The measurement of the size is performed using images from the camera and the subsequent analyses are done by the software.

Figure 2-12 *Zeiss Axio Imager M1.*

This instrument is used for:

- first evaluation of the quality of the intermetallic compound: homogeneity of the samples, presence of inclusions and undesirable phases;
- samples selection for the FDSC analysis.

2.3 Scanning Electron Microscopy

The Scanning Electron Microscope (SEM) is a type of electron microscope that produces images of a sample by scanning the surface with a focused beam of electrons. These electrons interact with the atoms of the sample. From this interaction are produced: secondary electron, backscattered electrons, Auger electrons and X-ray [13].
These signals allow the analysis of surface topography and the composition of the sample. A JSM-IT 300 LV by Jeol is used for the analyses on β-Al_3Mg_2 samples.

2.3.1 Principles

The main SEM components include:

- Source of electrons;
- Column down which electrons travel with electromagnetic lenses;
- Electron detector;
- Sample chamber;
- Computer and display to view the images.

Electrons are produced at the top of the column (usually the source is incandescent Tungsten filament), accelerated down and passed through a combination of lenses and apertures to produce a focused beam of electrons which hits the surface of the sample.
The sample is mounted on a stage in the chamber area; both the column and the chamber are evacuated by a combination of pumps. The level of the vacuum depends on the design of the microscope. The position of the electron beam on the sample is controlled by scanning coils situated above the objective lens. These coils allow the beam to be scanned over the surface of the sample. The beam scanning enables information about a defined area on the

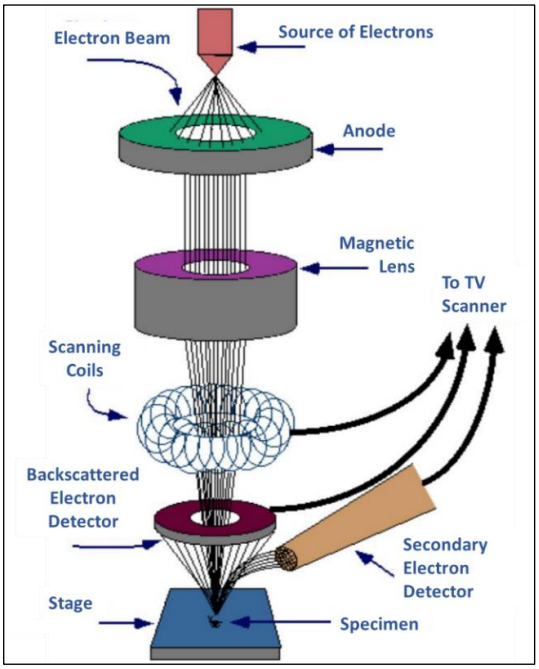

Figure 2-13 *Schematic representation of an SEM.*

sample; the maximum resolution provided by modern SEMs is between 1 and 20 nm. Because of the interaction between electrons and sample, the different type of signals written above are produced. These signals are then detected by different detectors as shown in Figure 2-13.

2.3.2 Energy Dispersive X-ray Spectrometry

Energy dispersive X-ray spectroscopy (EDS or EDX) is an analytical technique used for elemental analysis or chemical characterization of materials. X-rays, generated from the interaction between the electron beam and the sample, are used to perform this analysis.

When the sample is bombarded by the electron beam, electrons of an inner shell of the atoms are ejected from the atoms or promoted to higher energy shell. The resulting electron vacancies are filled by electrons from a higher state. The transition of an electron from a higher energy shell to the electron vacancy causes the emission of an X-ray, which energy is equal to the energy difference between the two electrons' states (Figure 2-14 a). The energy of the X-ray is characteristic of the element from which it originates.

The X-ray detector can measure the quantity of emitted X-ray and their own energy; when the X-ray hit the detector a charge pulse, proportional to the energy of the X-ray, is generated. Then the charge pulse is converted into a voltage signal. An analyser collects all the signals from the detector and it sorts them by voltage.

Then the data are plotted in an EDS plot (Figure 2-14 b); the spectrum of X-ray energy versus counts is evaluated to determine the elemental composition of the sample.

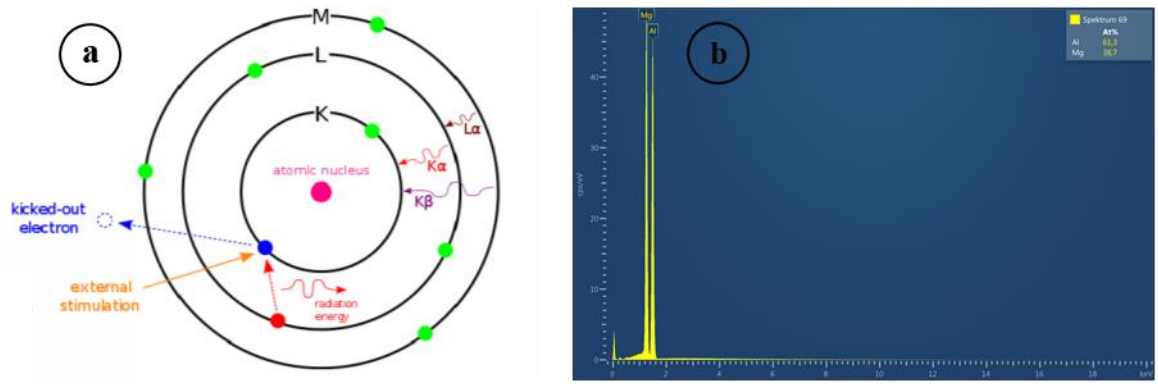

***Figure 2-14 a**) X-ray formation mechanism; **b**) EDS spectrum.*

3 Materials

This chapter describes materials, techniques and equipment used to produce the intermetallic compound Al_3Mg_2; further, there are explained the problems encountered and the way in which they are solved. In fact, the aim is to obtain a sample with the correct composition and free of impurities that could compromise the ability to carry out the thermal analyses using the Flash DSC 1.

3.1 Base materials

3.1.1 Metals

The production of the compound begins using high-purity metallic materials:

Table 3-1 *Materials used to produce β-Al_3Mg_2.*

Material	Purity [%]
Aluminium	99.92
Magnesium	99.90

According to Steuer (2007) [3], the objective is to obtain a sample with composition: 61.5% of Aluminium and 38.5% of Magnesium; this composition is within the range of existence defined by Okamoto (1998) [4]. However, for the preparation of the samples it is necessary to convert these values according to the weight percentages. The calculation procedure is shown using Eq. (3-1) and (3-2).

$$Al_{wt.\%} = \frac{Al_{at.\%} \cdot Al_{at.wt.}}{Al_{at.\%} \cdot Al_{at.wt.} + Mg_{at.\%} \cdot Mg_{at.wt.}} \cdot 100 = 63.9\ \% \qquad (3\text{-}1)$$

$$Mg_{wt.\%} = 100\ \% - Al_{wt.\%} = 100\% - 63.9\ \% = 36.1\ \% \qquad (3\text{-}2)$$

These weight percentage values are used for all the sample preparation according to the procedures that are reported in §3.2 .

Using Eq. (3-1) and (3-2) it is also possible to determine the range of existence of the intermetallic material in terms of weight percentage: β-Al_3Mg_2 exists for compositions between 62.5 and 64.9 wt.% of Aluminium.

Small rods and cubes of Al and Mg are obtained using a Struers SECOTOM-15/-50 cutting machine with a SiC cutting wheel. The average volume of the cubes is V = 8 mm^3; whereas the rods have the same section as the cubes (A = 4 mm^2) but they have a longer length: 10-35 mm. The oxide layer is removed from the surface of the pieces using sandpaper and then they are rinsed using iso-propanol to remove any residue.

In order to produce the desired compound, it is necessary to melt the pure metals and to obtain a suitable mixture while they are in the molten state; then the system could be cooled down to achieve the solidification. To protect metals from oxidation at high temperatures, which may occur in contact with air, the system must be in an inert atmosphere.

The inert atmosphere is made encapsulating the metals in a quartz glass tube as reported by Pogatscher (2014) [10]; the procedure is described below in §3.2.1

3.1.2 Quartz pipe

The pieces are small in size because they must be arranged inside a quartz glass tube with a circular section. The inside diameter of the tube is d_i = 10 mm, the external diameter is d_e = 12 mm and the length is about L = 200 mm.

The chemical composition of the commercially pure quartz glass has been taken from the technical data sheet of the product and it is shown in Table 3-2.

Table 3-2 *Chemical composition of quartz glass tube.*

Chemical element	Si	Al	Li	K	Na	Ca	Fe	Ti	Mg	B
Concentration (ppm)	> 97%	16	1.0	1.0	1.5	1.0	1.0	1.0	1.0	< 1.0

This type of pipe is chosen because it can be sealed using a blowtorch and it has also a high glass transition temperature ($T_g \approx$ 1200 °C); this temperature is considered sufficiently higher than the melting temperatures of Aluminium (T_m = 660.3 °C) and Magnesium

(T_m = 650.0 °C). So, it is expected that the pipe is able to hold the molten metal without softening or deforming.

Every tube is cleaned in order to avoid any kind of interaction between the liquid metals and the possible dirtiness inside the tube. At first the tubes are washed using tepid water and soap; then they are rinsed with deionised water and finally with iso-propanol.

3.1.3 Crucibles

In the first test the metal rods and cubes were simply putted inside the tube. But a reaction between Magnesium and Silicon occurred while the Mg was molten. For this reason, it is decided to try to insert the metallic material inside a crucible. In this way the metal would not touch physically the Silicon of the quartz tube and so the reaction between Mg and Si should not occur.

Considering the dimension of the quartz glass tube it is necessary to find crucibles with an external diameter sufficiently small to fit inside the tube, so smaller than 10 mm. At the same time the crucible should contains enough material to produce a substantial sample. Furthermore, the material of the crucible must be chemically inert with the metals.

Two solutions are applied; the materials that are tested for crucible applications are:

- Alumina (Al_2O_3): it is an Aluminium oxide; it is widely used due to its versatility and low material cost. It possesses a high melting point (T_m = 2050 °C), strong hardness and good chemical stability. It is chosen a crucible already available in the laboratory, the crucible supplied for the TGA analysis (Figure 3-1 a). The volume of material that it can contain is smaller than the amount charged in the other tubes; but it is considered enough for the subsequent tests since the FDSC requires very small samples. The internal diameter of the crucible is d_i = 4 mm and the height about h_i = 1.0 cm. The average amount of material (Al + Mg) inserted in the Alumina crucibles is 0.32 grams.
- Graphite (C): it is an allotrope of Carbon; it is a quite common type of crucible due to the good chemical inertia and the high temperature of melting. It is important to avoid the presence of Oxygen in the tube, otherwise it can burn at temperature higher than ≈ 500 °C. It is also very important to know that graphite is a conductor; therefore it interacts with the electromagnetic field generated by an inductor (one of the two heating methods used to obtain the melting of metals). They are made in

the laboratory of Metallurgy Department of Montaniniversität Leoben (Figure 3-1 b). Being tailor-made, it is possible to define the height of 4.0 cm. This crucible is bigger than the previous one: internal diameter d_i = 6 mm and free height inside h_i = 3.5 mm. This allowed an average amount of material (Al + Mg) in the crucible about 0.97 grams.

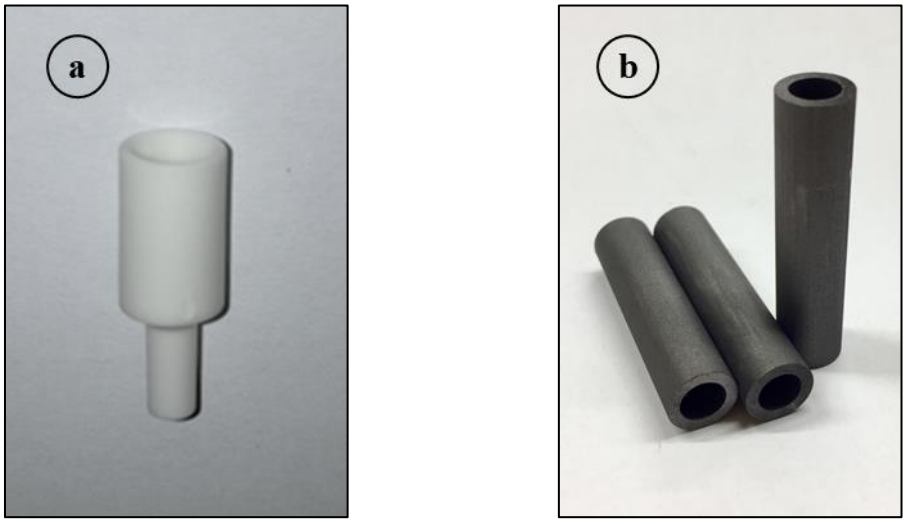

Figure 3-1 *Crucibles:* ***a)*** *Alumina (Al_2O_3);* ***b)*** *Graphite (C).*

3.2 FDSC sample production

3.2.1 Al_3Mg_2 production

The pieces of metal are weighted considering the percentage evaluated in §3.1.1 ;
As it may have been previously guessed, the tubes are filled with three different setups:

- Without crucible;
- With Alumina crucible;
- With Graphite crucible.

Two examples of the setups are given in Figure 3-2 and Figure 3-3. It is possible to see the different amount of material in the different setups (in the second picture the material is inside the crucible). The material is located in the closed edge of the tube (see *zone for material arrangement* in Figure 3-2).
The second step carried out to produce Al_3Mg_2 is the sealing process. It is necessary to make an inert atmosphere inside the tube to avoid reaction between the hot or molten metal

and Oxygen. A vacuum pump is connected at the open edge of the tube (see *vacuum pump connection zone* in Figure 3-2). The tube of the pump is connected to a three-way valve. It allows to empty the tube till 200 mbar; then, switching the valve, the glass tube is purged with Argon (5N purity). The filling-emptying procedure is repeated 5 times in order to assure the minimum possible amount of Oxygen inside the quartz tube, and perhaps the presence of a minimum amount of Argon, that is an inert gas.

While the vacuum pump is still working, a blowtorch is approached to the so-called *heated zone* (Figure 3-2). In this way just the central portion of the tube is heated by the flame; the material and the rubber tube of the vacuum pump are not heated up. The glass tube must be heated very carefully and slowly, so the change in viscosity is homogeneous and not pinpointed. While softening, the tube collapses due to the inside low pressure. At the appropriate time the tube is switched to ensure a good sealing in the central part of the tube. After the procedure, the part of the tube containing the material could be considered in an inert atmosphere with a low pressure.

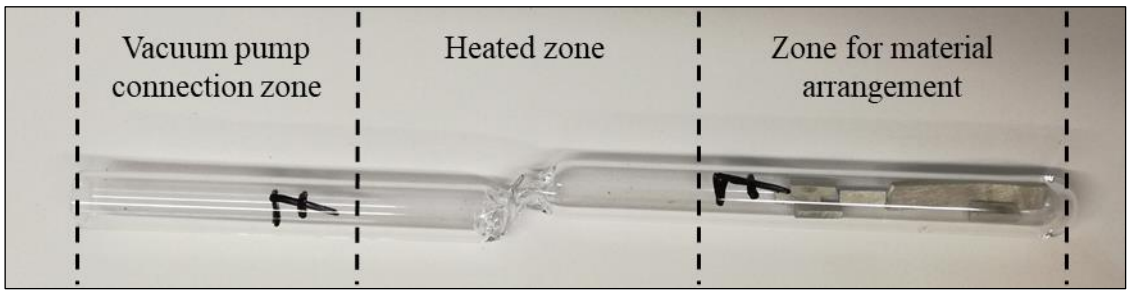

Figure 3-2 *Sealed quartz tube without crucible; different zones are defined.*

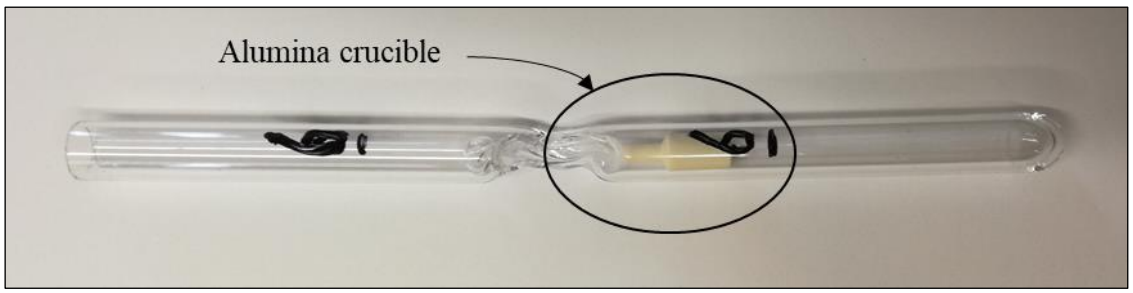

Figure 3-3 *Sealed quartz tube with Alumina crucible.*

Iso-propanol is used to verify that the two parts of the pipe are not connected. Some samples are discarded because some iso-propanol flows from the open edge to the *zone for material*

arrangement through the sealed zone. As the liquid, also the Oxygen could flow inside; so the samples are discarded: the glasses are broken and the metallic material reused.

After the sealing process the samples considered to be good moves to the last step of the Al_3Mg_2 production: the melting.

A first attempt is made in a traditional oven. A sample without crucible is subjected to a temperature of 700 °C for five hours. At the end of the treatment the glass tube is completely shattered; the metal is not even molten, probably because a layer of oxide has formed on the surface of rods and cubes. So an inductor it is used to melt the metals in subsequent experiments. Usually the inductor is used to make thermal treatment on steel billets. So it is necessary to customize the fastening mechanism in a proper way for the glass tubes; in fact they are quite fragile, in particular because of the shape obtained as result of the sealing process. One picture of the inductor and two pictures of the instant the metal is melted are given in Figure 3-4. Because of the particular process configuration and the fragility of the glass tubes, some pieces brake also during the melting step.

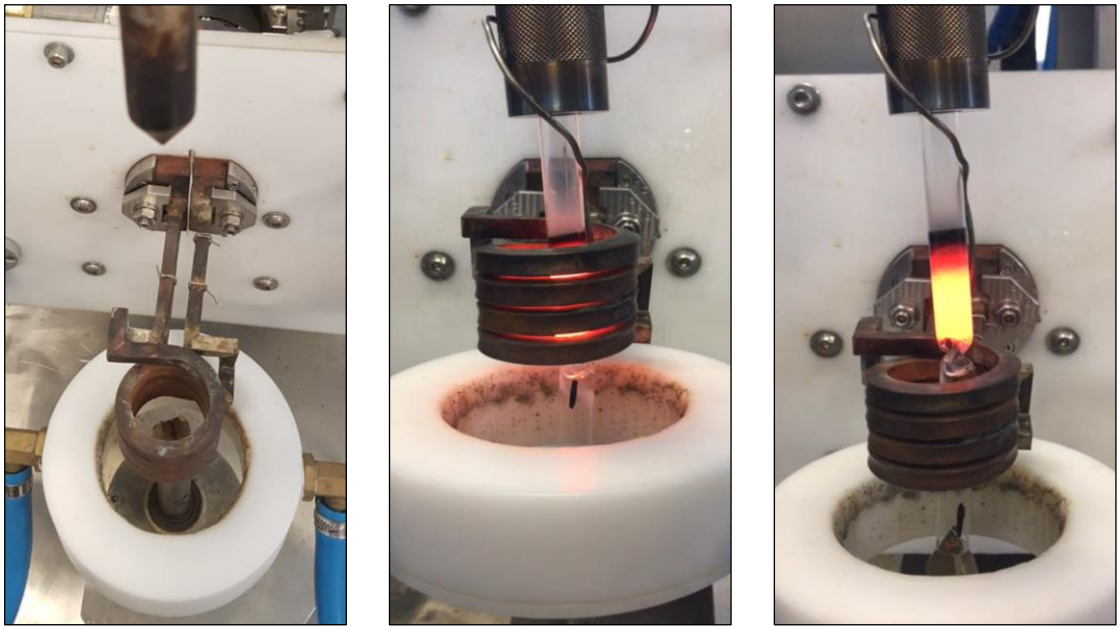

Figure 3-4 *Picture of the inductor and pictures of the tube with the molten material inside.*

The machine is able to melt the metal in few seconds; then it is decided to wait for a couple of minutes to ensure the homogenization of the liquid.

So the results of the melting process with the two different procedures show that the use of a traditional oven is not a good solution; good results are obtained with the induction machine instead.

In Figure 3-5 (a) it is shown the sample extracted from the tube placed in the traditional oven; the pieces of metal did not melt and a white Magnesium oxide has formed on the surface.

It is not been possible to melt the metal pieces inside the Alumina crucible (Figure 3-5 b), probably because the difficult interaction between the material and the electromagnetic field generated by the inductor; for this reason the idea to use the Al_2O_3 crucible for the production of the material is discarded.

Lastly, the samples without the crucible and the samples with the Graphite crucible have given, apparently, an alloy with good quality. The tubes are broken to take the material inside; a characterization analysis of the material is done to evaluate its composition and homogeneity. Figure 3-5 (c) shows how the crucible appeared after it has been cut to remove the material from inside.

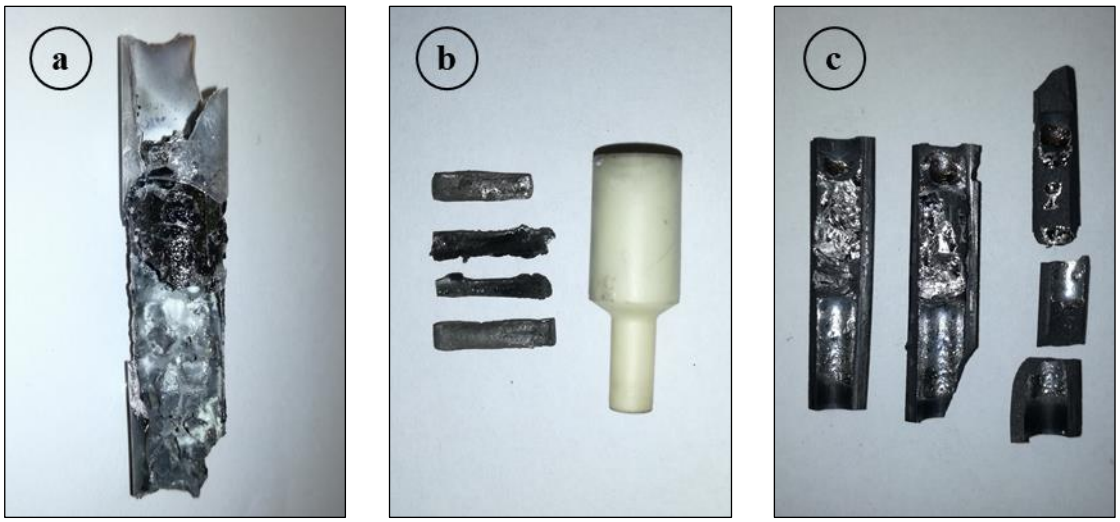

Figure 3-5 *Samples;* ***a****) discarded material from melting test in the traditional oven;* ***b****) pieces that did not melt in the Alumina crucible;* ***c****) cutted Graphite crucible with homogeneous intermetallic compound inside.*

3.2.2 Specimens production for OM and EDS analyses

The samples that has been produced with the method described in the previous paragraph are analysed with OM and SEM; the first one allows a simple and fast visual analysis to identify the presence of macroscopic inhomogeneities; it is also necessary to evaluate the quality of the samples for the subsequent SEM analysis. The second one has the objective to identify the chemical composition of the material; this allows to be sure to analyse samples with the correct composition in the Flash DSC 1.

Small amount of material, coming from different samples, are embedded in a polymeric resin. The reticulation of the resin takes 3 days and it is done in a box with controlled temperature and humidity. The embedded samples are polished using a grinding and polishing machine Struers Tegramin 30. The samples are mounted and then they are automatically polished.

Grinding papers are used to grind the material, to remove defects on the surface and to obtain a flat surface for optical analysis. A flow of water flows on the rotating plate to cool down the temperature and to remove residues. The abrasive paper is arranged on the rotating disk. Abrasive papers are classified by coarseness using numbers; the higher the number, the lower the abrasiveness. For high number of grits the average dimension of the SiC particles is low as shown in Table 3-3.

Table 3-3 *Grit designation and particles diameter.*

Grit designation	Average particles diameter (μm)
240	58
400	35
800	22
1200	15
2400	12

The samples are polished using papers with decreasing coarseness, up to paper with grit designation number 2400; this allows to obtain samples with polished surface. Between the change from a sandpaper wheel and the subsequent one , the samples are flushed with iso-propanol to remove residues and dried.

The quality of the polishing procedure is improved using OP-S Suspension by Struers; it is a colloidal silica suspension used for final polishing.

On samples produced for OM analysis a chemical attack is done; this allows to better see the presence of different phases and inclusion in the samples.

The etching method described by Buczynski, Kelly (2018) [18] is used. They used a 10% phosphoric acid solution for etching on β-phase; the samples were submerged in the solution for 45 seconds at 55 °C.

A simple system, shown in Figure 3-6, is prepared to do the etching procedure. A small container with the solution is positioned on an electric heater. A thermometer is used to check the temperature of the solution.

Figure 3-6 *Instrumentation for etching method.*

3.3 Difficulties

There were many difficulties during β-phase production that forced to try many configurations as explained in §3.1.3 . These difficulties were in particular about the production procedure. In fact, there were many critical steps as the sealing of pipes and the melting. The heating of the quartz is really difficult because the setting of the blowtorch is manual. This implies the fact that every time a tube is sealed the temperature of the flame is potentially different. Because of this variable, to produce about 10 well sealed tube, at least 15 tubes were discarded; some of the tubes were discarded because they were not well sealed after the process, and so the atmosphere was not inert as established. Some others instead reached too high temperature in localized region; this has led to the formation of bubbles in the inside of the pipe due to the low pressure imposed by the pump. The bubbles exploded and so, also in this case, there was no longer an inert atmosphere inside the tube. Another trouble, as already mentioned, was about the heating system used to melt the metals inside the tube. The traditional oven immediately showed to not be suitable for the procedure. Indeed, even if the slow heating rate, the tube shattered and the metals were not melted even after hours of heat treatment. The tube rupture could have been caused also by the tensions induced by the tube closing process. Anyway, it has been decided to use the inductor to melt the materials. This method indeed allowed to watch the tube and the material during the process. In this way the metals are monitored during the melting.

Also the induction melting had some problems: it was difficult to modulate the power of the inductor and also to check the temperature of the melted metals. Furthermore, it has not been possible to melt the samples inside the Alumina crucible as shown in Figure 3-5 b; the reason could be that the amount of material was too low to interact with the electromagnetic field.

The last problem was about the composition of the material. In particular, in samples obtained in the tubes without the crucible, unexpected crystals have been found.

The interaction between Magnesium and Silicon from the quartz pipe was not expected. The samples were characterized by the diffuse presence of inclusions. In order to understand the reason of the crystals a thermodynamics analysis was performed using FactSage software. A graphical representation of the system is shown in Figure 3-7.

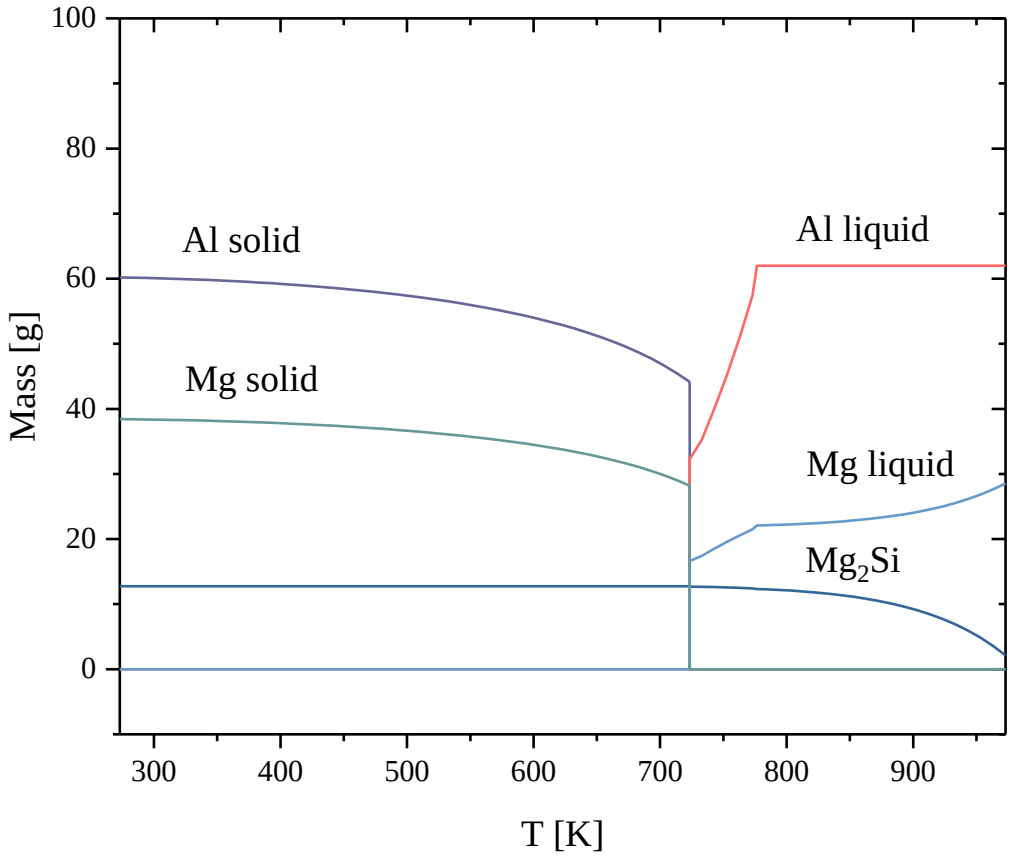

Figure 3-7 *Results from a thermodynamic analysis with FactSage.*

Assuming the presence of 60 g of Al, 40 g of Mg and 10 g of Si, it was demonstrated that the formation of Mg_2Si is thermodynamically predicted. Analyses on this compound with OM and SEM are reported in the results.

4 Results

The scope of this final chapter is to report all the results that are obtained. At first there is a focus on the results from the characterization of the material; the analysis with DSC, OM and SEM permitted to verify the microstructure and the composition of the produced samples. Then, there is a deep report about results from the Flash DSC; they are the core of this work. Many different time-temperature programs are performed in order to analyse phase transitions of the intermetallic compound. The presence of an unexpected solid-solid transition is identified; it is analysed in different ways.

4.1 Material characterization

All the samples that were appropriately melted in the tubes were subsequently handled to produce specimens for optical and electronic microscopy analyses. It was not possible to melt rods and cubes inside the Alumina crucible, consequently there are not results about the characterization of that material. After many attempts three samples are obtained: two with the configuration without crucible and one from the quartz tube with the Graphite crucible. In particular two different specimens are extracted from the last one; so a total of four samples are prepared. They are identified in the following results description as shown in Table 4-1.

Table 4-1 *Specimens identification.*

Setup	Specimen number	Identification
Without crucible	1	WC1
Without crucible	2	WC2
Graphite crucible	1	GC1
Graphite crucible	2	GC2

In order to follow the applied flow of the process it is decided to present the results dividing them according to the different setups. So, there is at first the description of results obtained from the analyses without crucible and then the description of results from setup with the Graphite crucible.

4.1.1 Without crucible setup

It has been previously written that the configuration without crucible has presented some problems. Unlike what was assumed, a reaction between the Magnesium and the Silicon from the glass tube occurred; this implies the presence of a secondary phase in the sample.

4.1.1.1 OM analysis

The first analysis with optical microscope shows the presence of an unexpected secondary phase in the Al-Mg alloy matrix. For WC1, two images of the crystalline structure are taken with the camera. They are showed below in Figure 4-1 (a) and (b); the image (a) is taken with 10x magnification, while image (b) is characterised by 50x magnification.

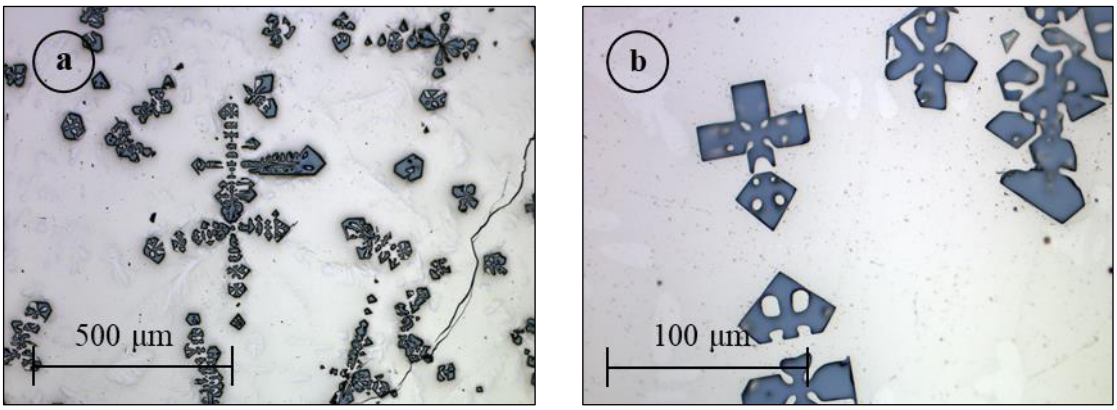

Figure 4-1 *Images of sample WC1 from OM analysis;* ***a****) 10x magnification;* ***b****) 50x magnification.*

It is possible to see that the crystals have an elongated shape and many preferential directions of growth, like dendrites. In the analysed samples, crystals have a length between about 10 and 500 µm. Figure 4-1 (b) shows a detail of the characteristic geometrical shape of the secondary phase. This sample was not etched, so it is not possible to see microstructure and grains of the Al-Mg phase, but just the presence of two different phases.

The second sample obtained without crucible is WC2; in order to try to avoid or reduce the reaction between Magnesium and Silicon, more power was supplied through the inductor; this allowed to reduce the time spent at high temperature. As soon as the metal was melted, the inductor was switched off to obtain the solidification of the material. The idea was to minimize the time for the interaction between the two substances. This was not satisfactory; it is possible to see in Figure 4-2 that the secondary phase is still present.

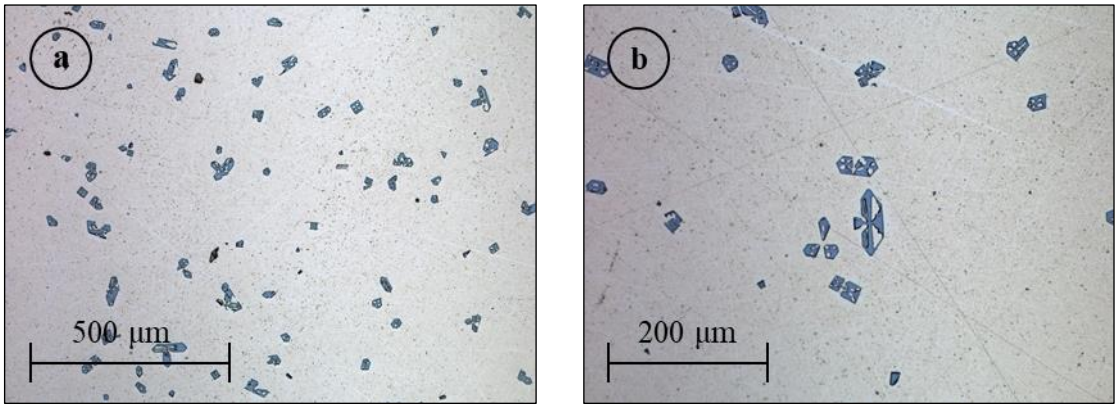

Figure 4-2 *Images of sample WC2 from OM analysis;* ***a)*** *10x magnification;* ***b)*** *20x magnification.*

Neither this sample was etched. There are many scratches on the surface of the sample, probably due to the polishing process.

Actually, the amount of secondary phase is less than the previous sample (WC1), but it is still present. In specimen WC2 the dimension of the secondary phase is smaller than in sample WC1. In this case the dimensions are between about 10 and 70 µm.

4.1.1.2 EDS analysis

EDS analysis with Scanning Electron Microscope was carried out to analyse the composition of the matrix and the secondary phase in sample WC1. This step was fundamental for the advancement of the thesis work. It allowed to determine the cause of the secondary phase; afterwards it was possible to introduce the use of crucibles in order to avoid its presence.

Two different representation of the EDS analysis are reported.

In Figure 4-3 it is possible to see the magnification of an area with the secondary phase in the middle.

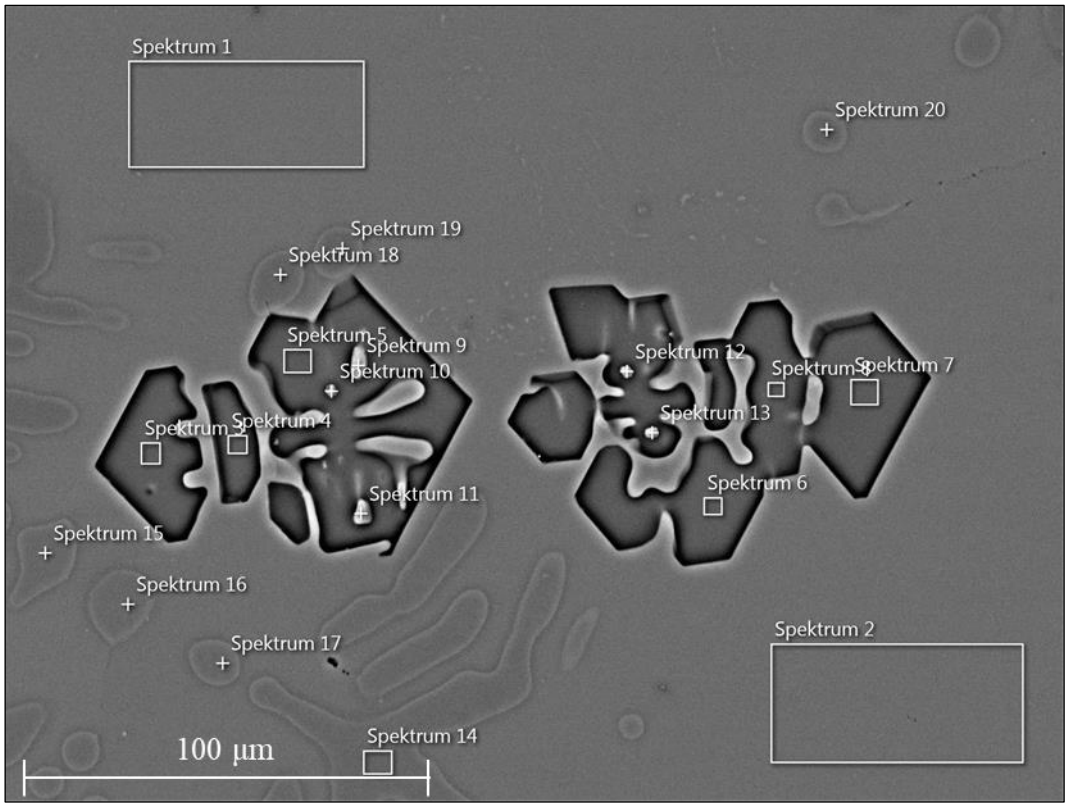

Figure 4-3 *SEM image for EDS analysis of WC1.*

Many spots and areas are analysed; this allows to understand the overall composition and also to compare the composition featured in different zones of the sample.

All the measurements are reported in Table 4-2. It is possible to see that the composition in spectrum 1 and 2 (these are the analyses of homogeneous areas) are equal. This means that the Al-Mg matrix is almost homogeneous. The measured compositions are within the range of existence for Al_3Mg_2 (between 37.5 and 40 at.% of Magnesium).

From the analysis of other zones, it is clear that the composition is quite changeable. Some points show the simultaneous presence of Al, Mg and Si; except in spectrum 9 and 11 which have an Aluminium percentage respectively of 13.1 at.% and 10.7 at.%, the atomic percentage of Al is smaller than 2.7 at.%.

Differently, the evaluated zones just composed by Mg and Si present a homogeneous composition. The average percentage is 69 at.% of Magnesium and 31 at.% of Silicon. The secondary phase is determined to be Mg_2Si, as already mentioned in §3.3 .

It is also important to underline that in some measurements (14, 15 and 16) the composition is free of Silicon, but the atomic percentage of the alloy does not fall within the range of composition for Al_3Mg_2.

***Table 4-2** Atomic percentage composition from EDS analysis on WC1.*

Spectrum	Al [at.%]	Mg [at.%]	Si [at.%]
1	60.5	39.5	-
2	60.5	39.5	-
3	2.7	66.6	30.7
4	1.5	30.9	67.6
5	-	70.3	29.7
6	-	68.6	31.4
7	-	68.5	31.5
8	-	68.4	31.6
9	13.1	55.5	31.4
10	1.1	68.0	30.9
11	2.0	66.9	31.1
12	-	68.3	31.7
13	10.7	62.6	26.7
14	80.6	19.4	-
15	79.3	20.7	-
16	79.6	20.4	-
17	61.8	38.2	-
18	64.0	36.0	-
19	61.3	38.7	-

The other output obtained from the EDS analysis are the EDS maps showed in Figure 4-4. In these maps the coloured dots represent the presence of a specific element in the sample. In the description of the figure it is possible to see which chemical element the different maps refer to. The dark zones represent the areas where the element is not present.

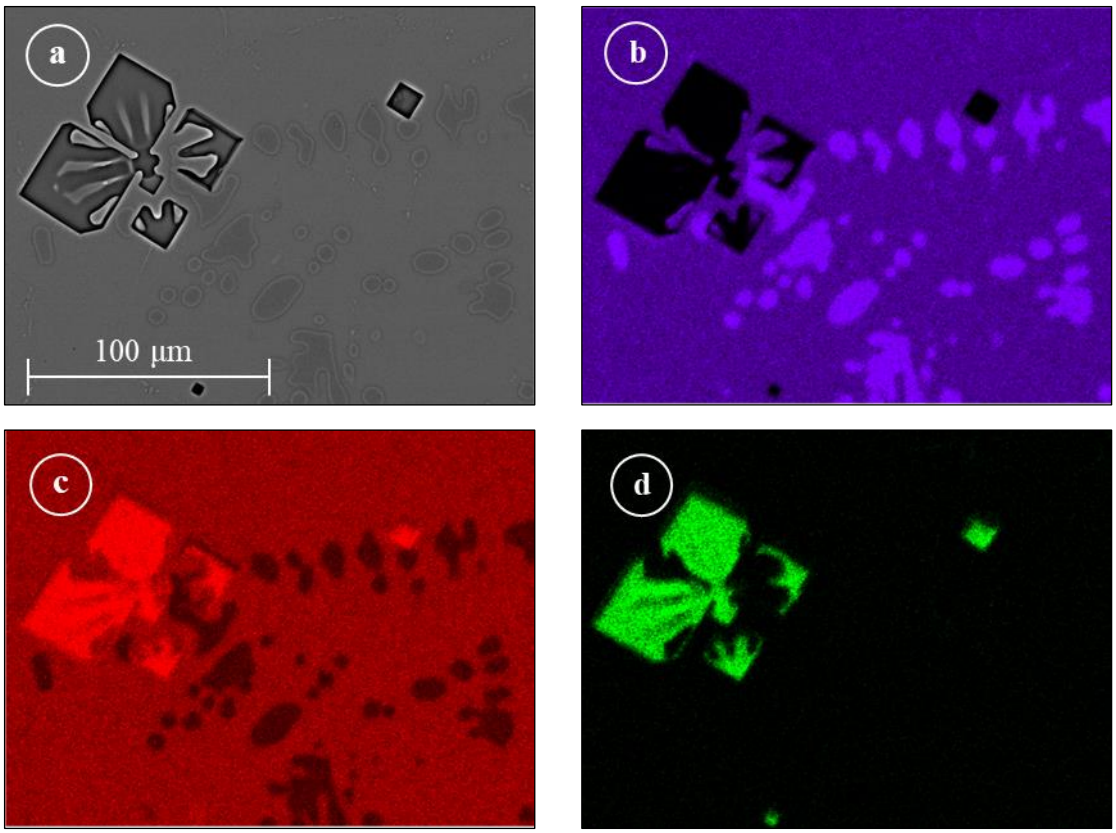

Figure 4-4 *EDS maps of element distribution on sample WC1;* ***a****) magnification of the sample;* ***b****) Aluminium map distribution;* ***c****) Magnesium map distribution;* ***d****) Silicon map distribution.*

From this kind of picture it is easy to confirm that the secondary phase is just the result of the reaction between Magnesium and Silicon. It is also possible to say that the Silicon did not interact with the Aluminium; indeed, Figure 4-4 (b) and Figure 4-4 (d) seem to be complementary.

Even if the matrix is composed by Al_3Mg_2 it is not possible to use this sample for further analyses with Flash DSC 1 because it is not possible to know if the secondary phase could influence the measurements. For this reason, no DSC or FDSC analyses are performed on these samples. The description of results proceeds with samples from Graphite crucible configuration.

4.1.2 Graphite crucible setup

After the melting process, the Graphite crucible is extracted from the quartz tube. In order to remove the material from the crucible it is necessary to cut it as shown in Figure 3-5 (c). The material inside looks brittle and porous. Indeed, during the melting process, it was possible to watch the liquid metal boiling.
Two samples are taken end embedded for further analyses. Sample GC1 is taken from the bottom of the crucible, while GC2 is taken from the top.

4.1.2.1 OM analysis

GC1 specimen is etched in order to better show the microstructure of the sample. It is characterized by the presence of two different phases (Figure 4-5). In particular, it is possible to see a main phase (the clear one) and a secondary phase between the grains (lamellar structure). The grains of the main phase have a dimension about 20-30 μm. The secondary phase looks to have a lamellar structure, as it happens in a eutectic system. So the system is inhomogeneous and it is not expected to have the right composition necessary for further analyses with Flash DSC 1. Anyway, it is analysed with SEM to understand the characteristics of the composition.

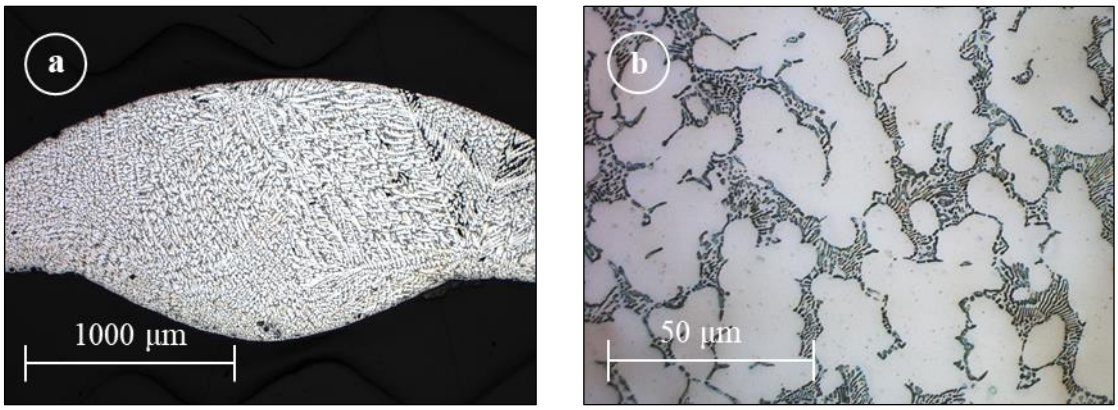

Figure 4-5 *Images of sample GC1 from OM analysis;* ***a****) 5x magnification;* ***b****) 50x magnification.*

Also GC2 is etched; in this case the composition looks to be more homogeneous (Figure 4-6). The grain boundaries are not easy to see, neither with high magnification in Figure 4-6 (b). Anyway, it is possible to see just one phase. This mean that it could be a sample with the right composition. In Figure 4-6 (a) it is possible to see black regions; these areas

are just porosities in the specimens probably caused by the boiling in the liquid metal during the melting. Also in Figure 4-6 (b) it is possible to see some inclusions that are characterized in the following paragraph with EDS analysis.

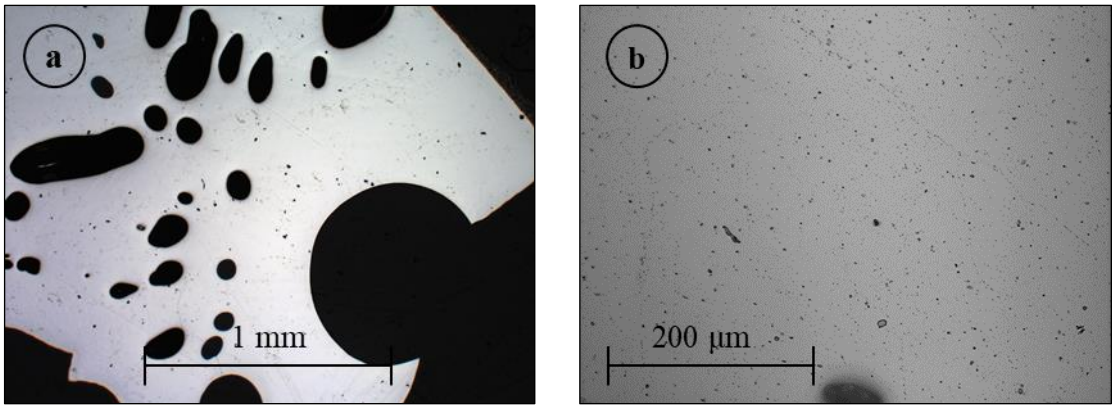

Figure 4-6 *Images of sample GC2 from OM analysis;* ***a)*** *2.5x magnification;* ***b)*** *20x magnification.*

4.1.2.2 EDS analysis

The sample GC1 is analysed with SEM in order to evaluate the composition of different phases present. The analysed areas are shown in Figure 4-7 and all the concerning measurements are reported in Table 4-3.

It is important to underline that, unlike what happened in the case of setup without crucible, with this configuration the only elements present in the sample are Al and Mg. This means that the use of the Graphite crucible is essential and successful to avoid the reaction between Magnesium and Silicon from the quartz tube. It is also important to verify that there are no traces of Carbon from the crucible.

Unfortunately the evaluated composition for GC1 is not homogeneous and not even in the right range. The average composition measured in the clear areas is about 63.2 at.% of Mg; whereas in the secondary phase the average composition is 72.0 at.% of Mg. This means that, although efforts were made during the melting process to keep the material in the molten state for a long time in order to facilitate mixing, it was not enough in the lower part of the crucible. For this reason the composition is inhomogeneous as to have a prevalence of Mg on the analysed surface.

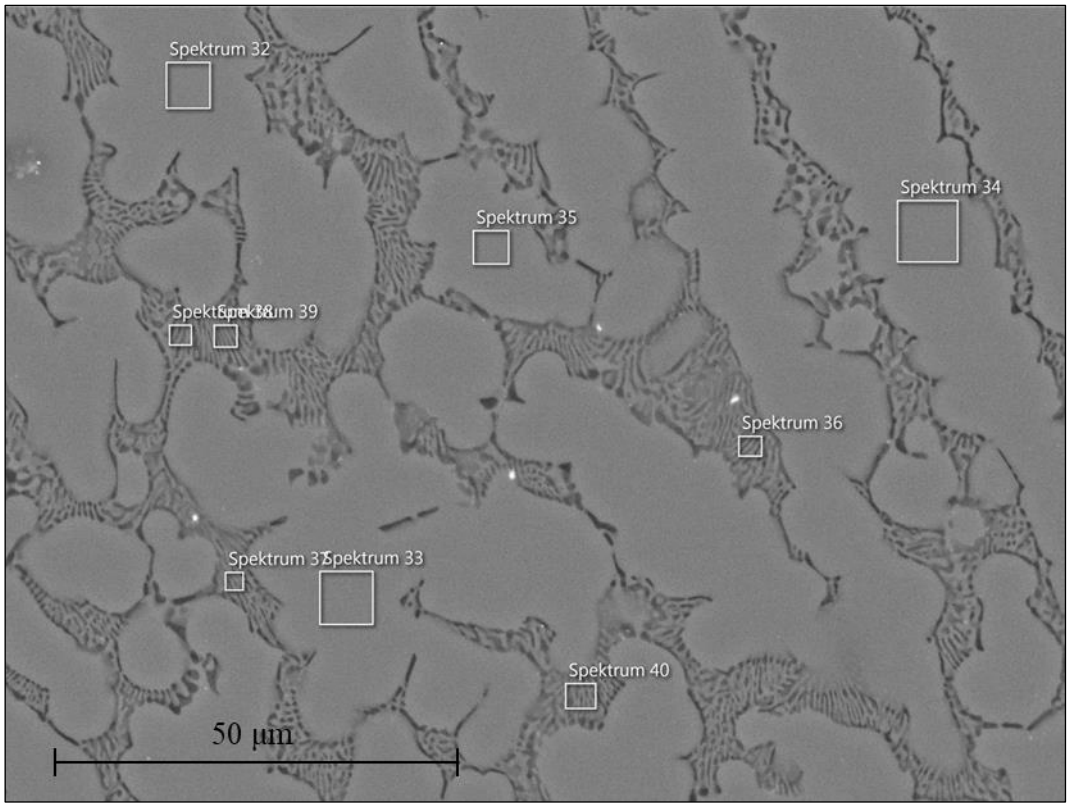

Figure 4-7 *SEM image for EDS analysis of GC1; magnification 1000x.*

Table 4-3 *Atomic percentage composition from EDS analysis on GC1.*

Spectrum	Al [at.%]	Mg [at.%]
32	36.6	63.4
33	37.0	63.0
34	36.7	63.3
35	36.8	63.2
36	28.5	71.5
37	28.3	71.7
38	27.4	72.6
39	27.5	72.5
40	27.7	72.3

Finally, also sample GC2 is analysed. It is possible to see in Figure 4-8 that the microstructure is homogenous. As already written above, there are some porosity in the sample, but this is not considered a problem for further analyses.

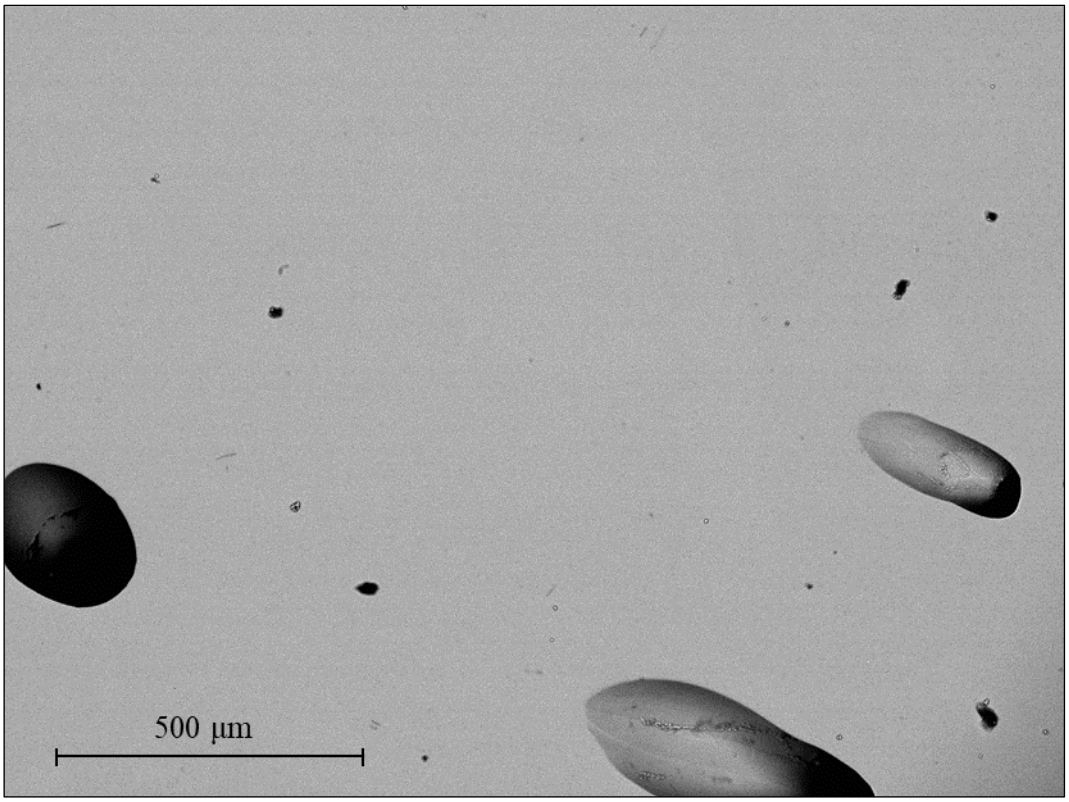

Figure 4-8 *SEM image of GC2; magnification 75x.*

The composition measured with EDS analysis on GC2 specimen is within the range of existence of Al_3Mg_2.

Few very small inclusions are identified on the surface and analysed. The inclusions are thin and with a length around 25 µm. Three of them are analysed with EDS technique; pictures are reported in Figure 4-9 and the related measurements are in Table 4-4. In particular, measurements 61, 62, 63 are related to (a), 67, 68, 69 to (b). and 70, 71 are related to (c). In all the cases the analyses of areas confirm the right composition of the sample. In case (a) the measurement on the inclusion show just a changing in the composition. In case (b) the presence of Oxygen is measured; this could be probably justified as a residue coming from the surface of rods or maybe the reaction with some residual Oxygen in the atmosphere. In case (c) a percentage about 70 at.% of Carbon is measured; this can be attributed to the Graphite crucible.

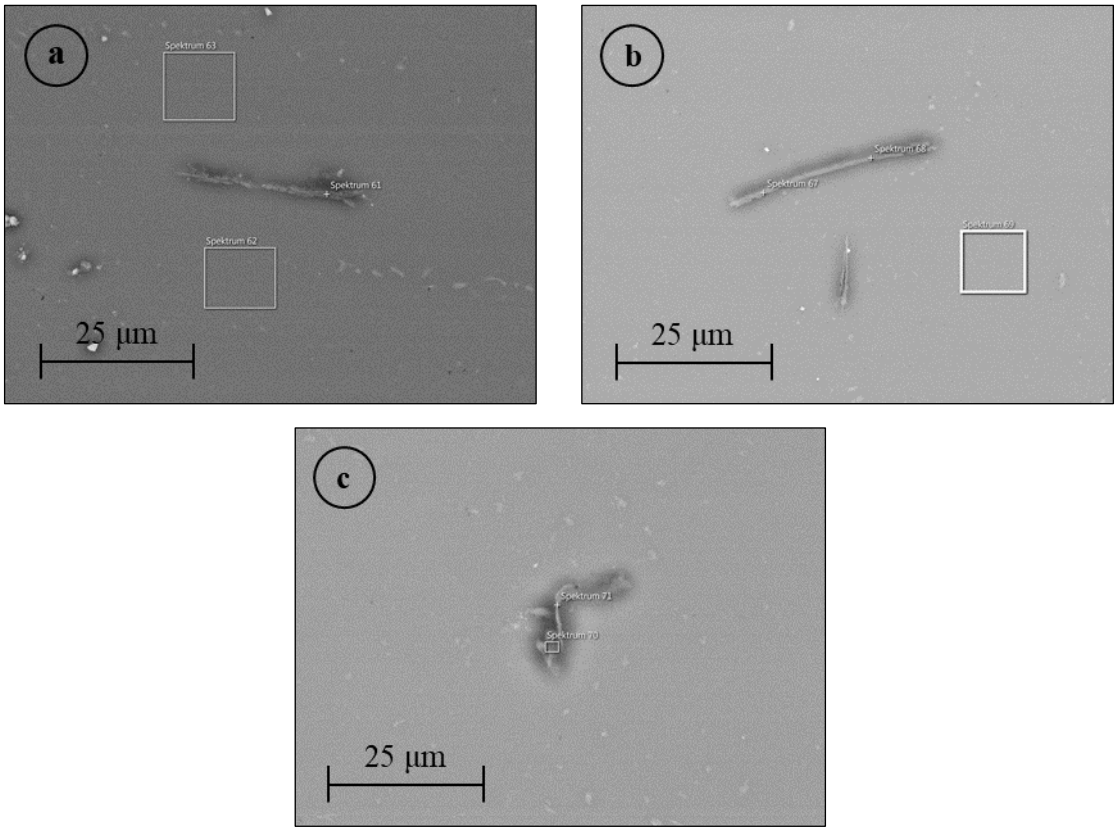

Figure 4-9 *SEM images for EDS analysis of GC2; magnification 1500x.*

Table 4-4 *Atomic percentage composition from EDS analysis on GC2.*

Spectrum	Al [at.%]	Mg [at.%]	O [at.%]	C [at.%]
61	69.8	30.2	-	-
62	61.6	38.4	-	-
63	61.4	38.6	-	-
67	55.6	20.6	23.9	-
68	58.9	22.6	18.5	-
69	61.3	38.7	-	-
70	18.1	14.4	-	67.6
71	14.9	12.4	1.3	71.4

Although the presence of small impurities on the surface of the sample has been verified, it is considered possible to proceed with the thermal analyses DSC and then FDSC.
For DSC analysis, the presence of such small impurities should not affect the measurement of the melting temperature of the sample, which has only a quantitative purpose.
For analysis with Flash DSC 1, samples are obtained only from areas of the surface where the inclusions previously identified are not present.

4.1.2.3 DSC analysis

The DSC analysis aims to characterize the sample also evaluating the melting temperature, which can be easily compared with the data reported in the phase diagram by Okamoto [4]. Furthermore, it allows to determine the enthalpy of melting; so then it will be possible to evaluate the mass of the samples analysed with the Flash DSC 1.
A probe whit mass = 0.00945 grams is positioned in the DSC instrument inside an Alumina crucible. A temperature program with constant heating rate 10 K/min is performed from room temperature till 770 K.
The graph obtained is shown in Figure 4-1.

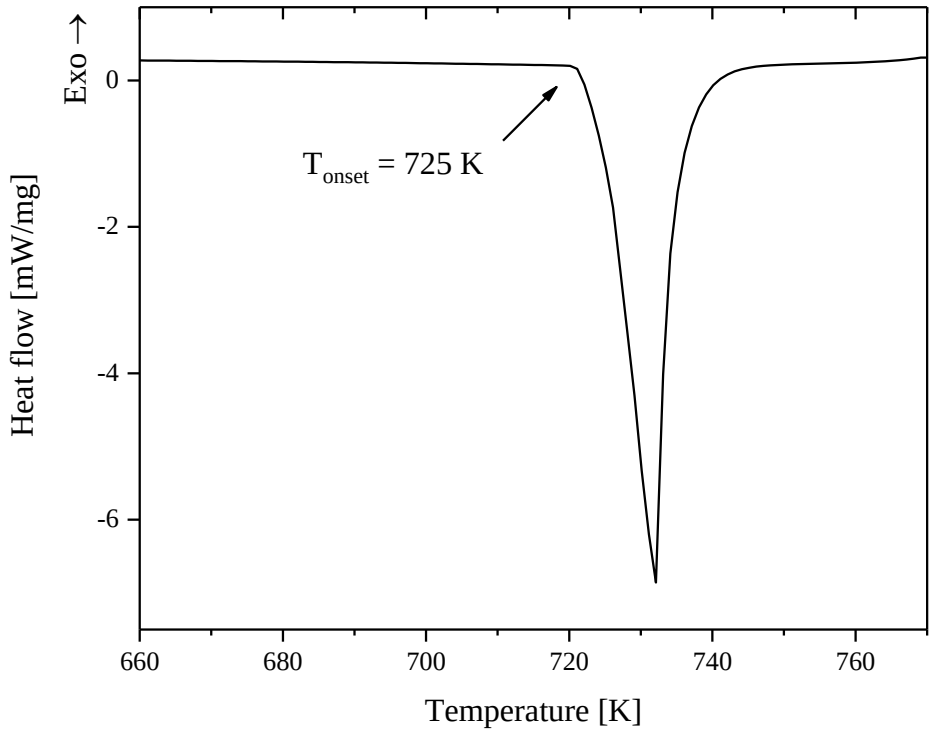

Figure 4-10 *DSC peak of melting.*

There is an endothermic event which correspond to the melting of the material. The evaluation of the melting onset temperature is carried out with the software and corresponds to T_{onset} = 725.85 K; this melting temperature correspond to the melting temperature reported in literature for Al_3Mg_2 [4].
The peak of melting has been integrated; since the mass of the sample is known, from this integral the enthalpy of melting of the intermetallic compound is obtained. From this analysis, the enthalpy of melting for Al_3Mg_2 results to be 287.9 J/g. Thanks to this value it is possible to measure the mass of samples in further experiments with Flash DSC 1.
At the end of the experiment the sample is strongly oxidized on the surface, therefore the cooling curve is not reported.

4.2 Fast Differential Scanning Calorimetry

After all verifications it is sure that the material from GC2 is Al_3Mg_2. So it is possible to proceed with the final analysis: the thermal analysis on Al_3Mg_2 with Flash DSC 1.
The use of material taken from the samples used for OM analysis ensures that there is a good contact between the sample and the chip membrane.
On some samples repeated cycles of melting and solidification are carried out. Samples are kept at a temperature higher than T_m even for few minutes in order to promote oxidation phenomena. After this test the samples show no change in the curves; the evaluated exchanged heat due to solidification and melting is always the same. This means that, thanks to the Argon flowing in the specimen surrounding, oxidation phenomena are inhibited. So it is possible to use every sample for many experiments.
It is found that the torque force with which the chip sensor is fixed is different each time the chip is positioned. This results in the formation of tensions in the chip membrane. Consequently, a shift towards more positive temperature values is displayed in the measurements. In order to solve this problem the *Temperature correction* function of STARe software is used. It allows to correct the measured temperature thanks to the melting temperature of reference materials such as Lead (T_m = 327.5 °C) and Zinc (T_m = 419.5 °C).
This is a brief description of the framework of the experimental process with FDSC.
Because of the small dimension of the specimens, a lot of sample are used for FDSC analysis; this is important especially in order to become familiar with the instrument. But the reported results are obtained just from 3 samples.

Their mass is calculated using the formula:

$$Mass = \frac{Energy\ of\ melting\ from\ FDSC\ analysis}{Enthalpy\ of\ melting\ from\ DSC\ analysis} \qquad (4\text{-}1)$$

The Energy of melting is determined just evaluating the integral of the melting peak from FDSC analysis curves.

The evaluated masses for the three samples are reported in the following table:

Table 4-5 *Mass of samples.*

Sample	Energy of melting [J]	Mass [g]
1	2.6E-04	9.03E-07
2	8.5E-04	2.95E-06
3	1.3E-04	4,52E-07

As already written in instrumental description, the weight of the specimens used in the Flash DSC 1 is very small. The smaller the sample size, and the higher the cooling speed applicable. But the smaller the sample size and the smaller the signal returned by the instrument. Therefore, samples with different sizes are used according to the performed analyses.

The aim of FDSC analyses is to analyse the complex intermetallic compound in non-equilibrium condition in order to try to obtain phases not foreseen by the Al-Mg phase diagram such as metastable or amorphous phases.

The first analysis just focuses on cooling intermetallic compound from the molten state to room temperature. Then the material is heated up again to the liquid state. The procedure is applied with different cooling rates in order to see if a high rate could change the behaviour of the solidification process.

As shown in Figure 4-11 and Figure 4-12, the sample is heated up till 760 K; then it is cooled down respectively at -50 K/s and -600 K/s. Finally the sample is melted again increasing the temperature at 50 K/s. The heating and cooling rates (Φ) just mentioned have been selected after many tests because they well represent the results here described.

In Figure 4-11 it is possible to see that the cooling curve is characterized by two exothermic peaks. The first one can be attributed to the solidification of the liquid intermetallic material because the T_{onset} of solidification is a bit lower than T_m = 725 K. The shift of the T_{onset} for solidification phenomena is due to the supercooling necessary to promote crystallization

processes. At a temperature about 675 K there is a second exothermic peak with smaller size. It corresponds to a solid-solid phase transition and it is not foreseen in the Al-Mg phase diagram. It cannot be the polymorphic transition because the temperature does not correspond. The two peaks have been integrated in order to compare their dimensions. The amount of exchanged heat of the second peak is about equal to 17.85% of the exchanged heat for the first, and bigger, peak. This evaluation has been made with samples with different dimension and the ratio is constant. The heating curve (50 K/s) after cooling at -50 K/s shows just an endothermic peak. It corresponds to a melting event and it happens at ~730 K. The melting temperature should be at ~725 K, but the temperature correction procedure is not that precise. Therefore, there remains a certain difference compared to the previously defined melting temperature.

The curves represented in Figure 4-12 are obtained with a cooling rate of -600 K/s (faster than the cooling rate applied in the previous analysis) and with a subsequent heating rate of 50 K/s (equal to the heating rate applied in the previous analysis).

These curves look different from the previous ones. In the cooling curve there is just one exothermic peak; this is the peak of solidification from melting. It is wider than the one obtained at -50 K/s because the faster the cooling is and the larger the solidification peak is. But the integral of the two peaks shows that the heat exchanged is the same.

The typical shape of the solidification peak caused by supercooling (see Figure 2-2) is easier to see in Figure 4-12 thanks to the faster cooling rate applied.

Instead, in the heating curve there are two peaks. The first, low and wide, appears at about 600 K; it is an exothermic peak. It is not foreseen from the Al-Mg phase diagram and, furthermore, it is not present either in the DSC curve or in the heating curve of Figure 4-11. The second peak corresponds to the melting peak already seen before.

The smaller endothermic peak present in the cooling curve of Figure 4-11 and the smaller peak present in the heating curve of Figure 4-12 are compared using the energy measured with the integration of the peaks. The result is that they look to represent the same solid-solid transition. This means that a solid-solid transition occurs while cooling down from the liquid for low cooling rates, but it could be avoided using high cooling rates; and if it is avoided while cooling then it occurs during the subsequent heating.

There are no traces of glass transition, even at high cooling rates.

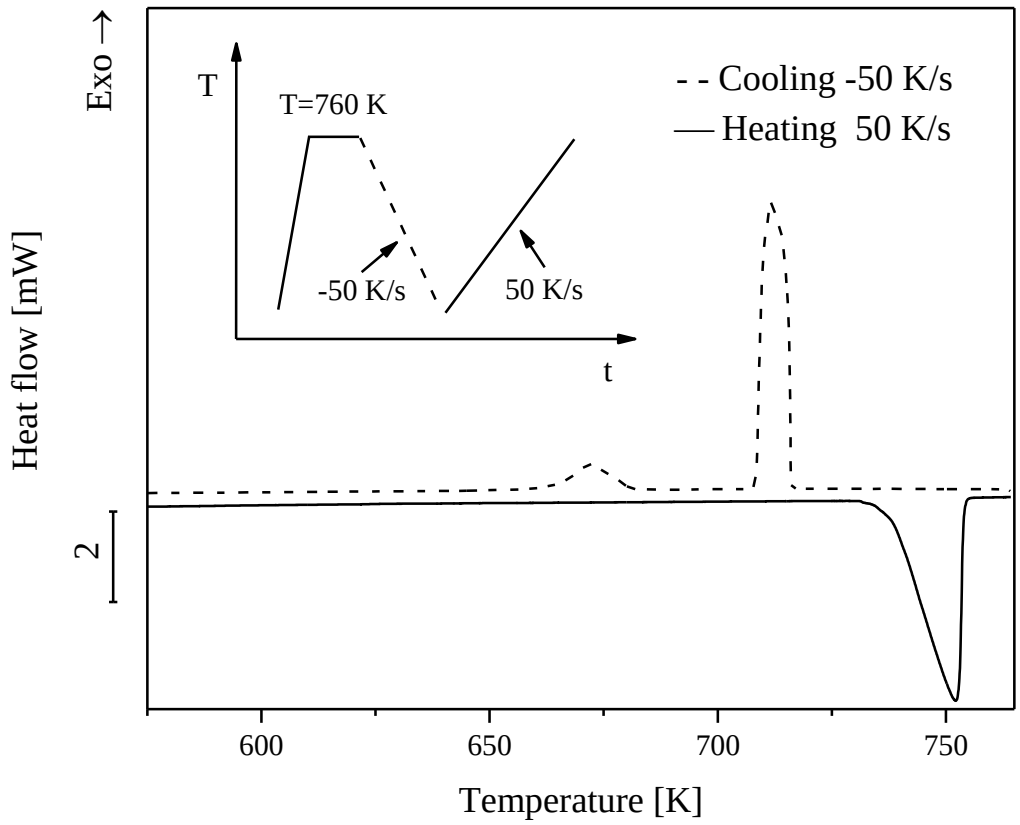

Figure 4-11 *FDSC curves: cooling (-50 K/s) and subsequent heating (50 K/s).*

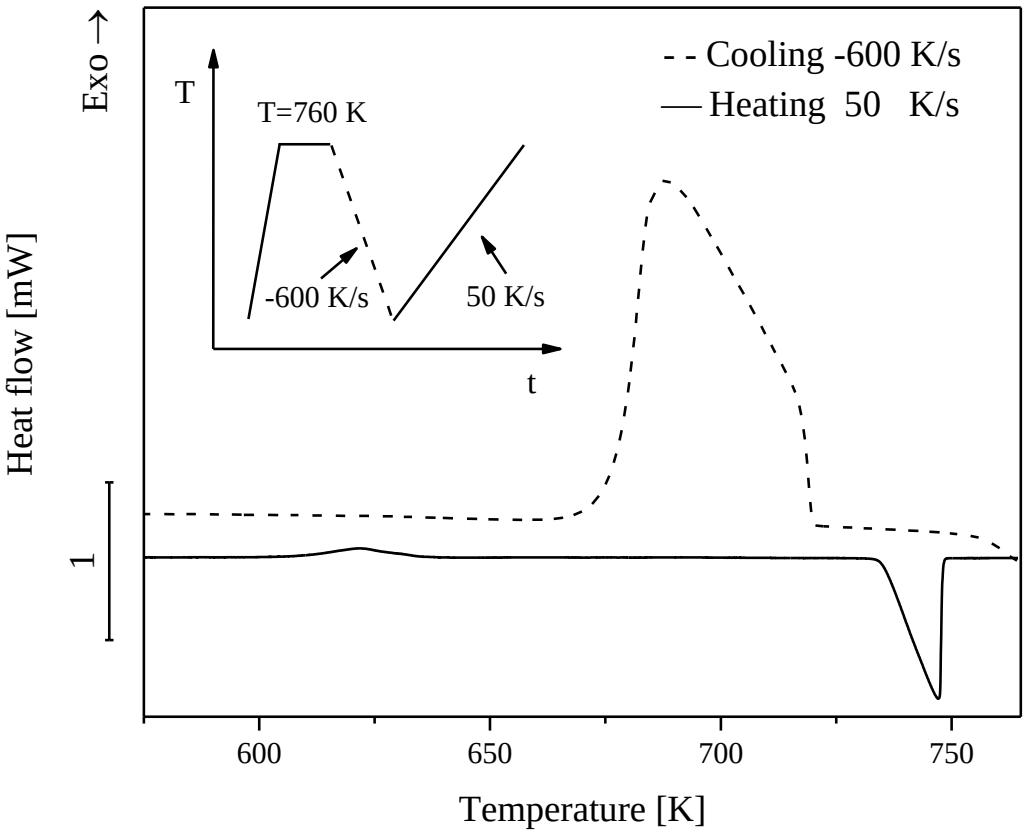

Figure 4-12 *FDSC curves: cooling (-600 K/s) and subsequent heating (50 K/s).*

The focus is therefore on the analysis of the solid-solid transition. A wide range of cooling rates is studied in order to explore the behaviour of this transition and to understand which is the lowest cooling rate required to prevent the transition while cooling.

The cooling rates between -50 and -650 K/s are analysed using step of 50 K/s. So in this graph only cooling curves are shown.

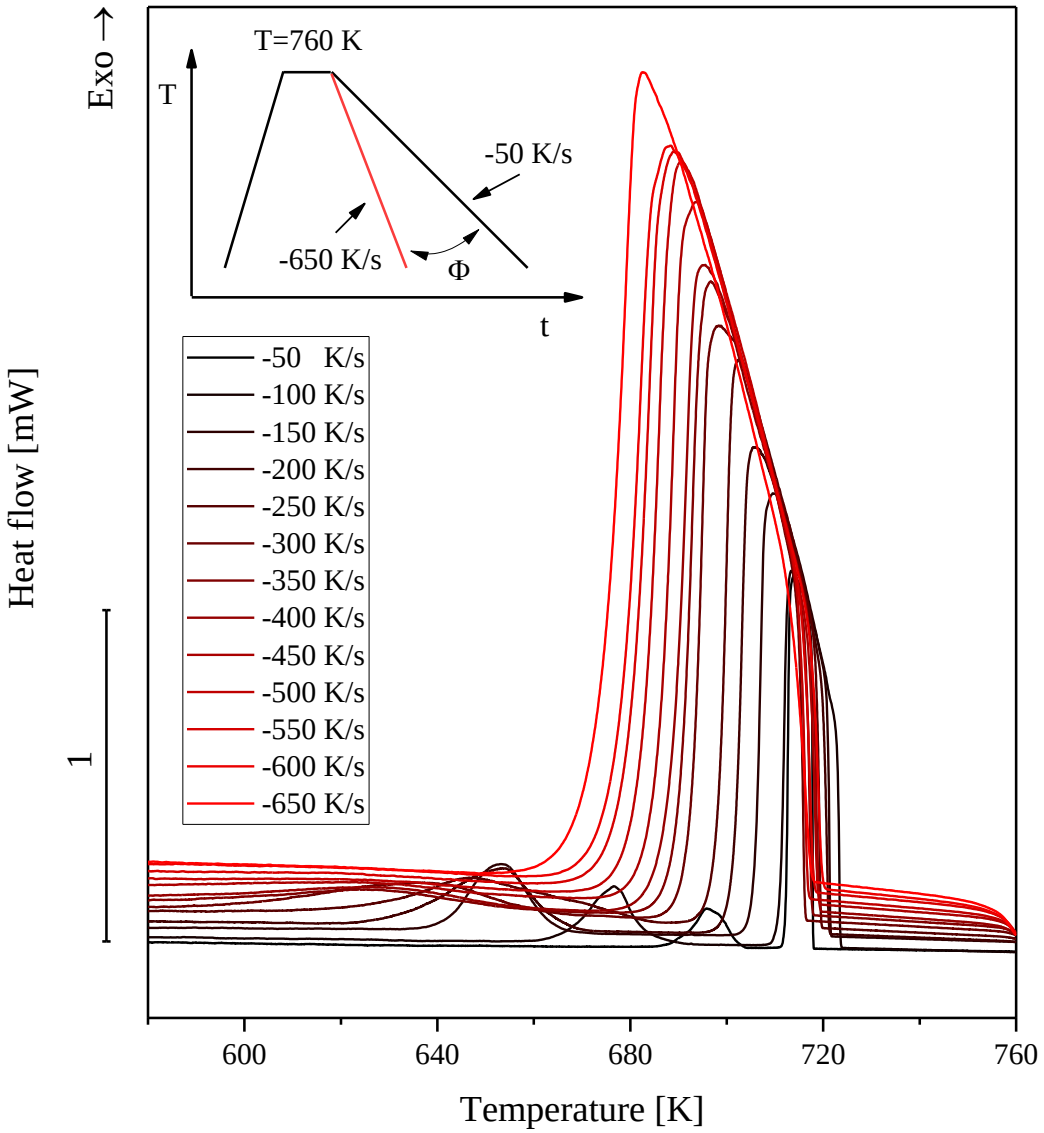

Figure 4-13 *FDSC curves obtained for cooling rates between -50 and -650 K/s.*

From black to red curves the applied cooling rate increase. As the cooling rate increases the peak of the solid-solid transition shift to lower temperature. Furthermore the shape become wider and flatter, starting from rate -200 K/s. The peak become flatter and flatter , until it completely disappears around -500 K/s. It is observed that as the shape of the peak varies, the solid-solid transition energy also varies. In particular, as the speed increases, the

released energy decreases. While observing a reduction in the released energy during cooling, a corresponding increase in the peak during heating can be seen.

This specific phenomenon is analysed and the results are reported in Figure 4-14.

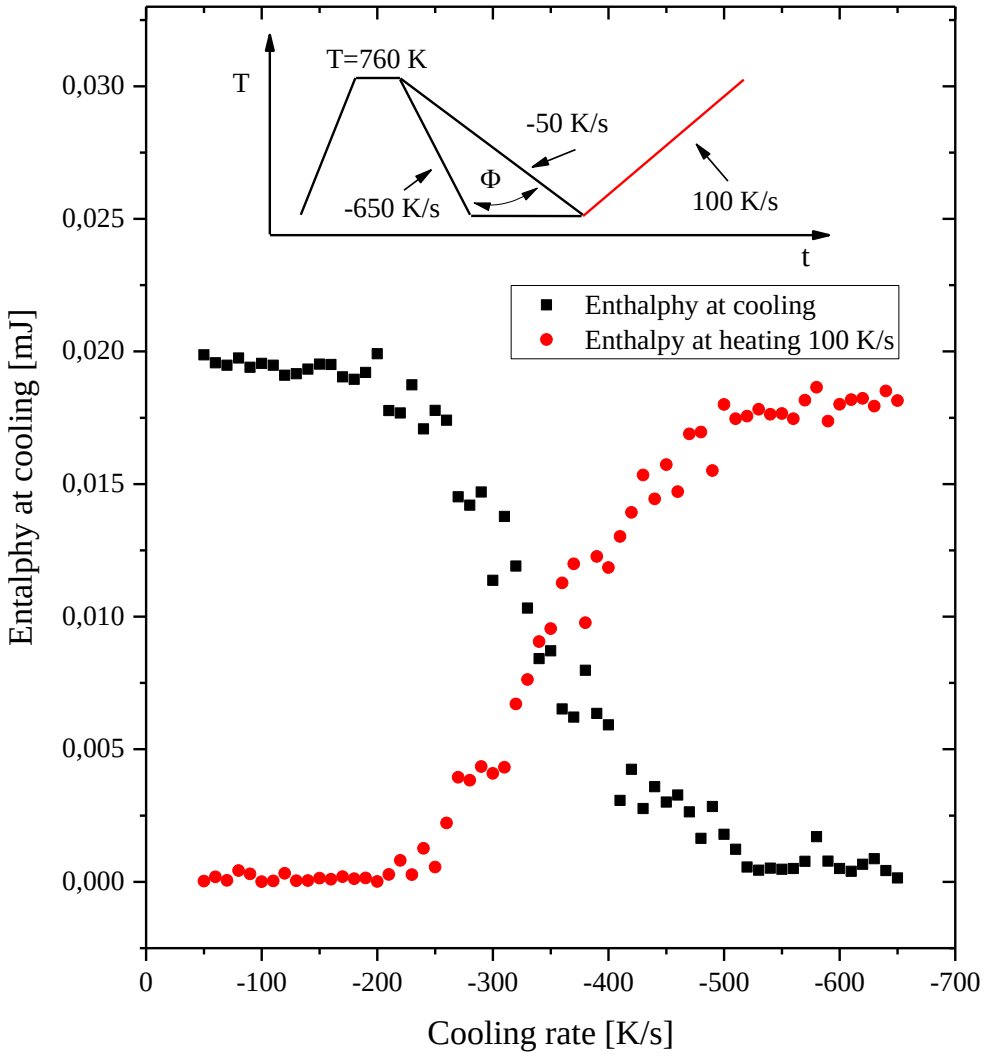

Figure 4-14 *Solid-solid transition peaks analysis for different cooling rates between -50 and -650 K/s.*

To the sample are applied cooling rates from -50 up to -650 K/s by intervals of 10 K/s (-50, -60, -70, …). The black squares (■) represent the energy released by the system (exothermic phase transition). It is evaluated again from the integral of the peaks on the cooling curves. It is possible to see that from rate about -200 K/s the measured energy released by the system for the transition decrease from the average value 19.63 mJ to 0 mJ. The values are around 0 mJ for cooling rates higher than -500 K/s. The energy released decreases linearly between -200 and -500 K/s. After the cooling, the sample is heated always with the same rate: 100 K/s. The reason of this stage is just to evaluate the released energy during heating, so it is possible to apply the same rate every time. The measurements

of the solid-solid transition peak are represented by the red dots (●). As the released energy in the cooling curves starts to decrease (for increasing cooling rate) the released energy in the respective heating curves starts to increase. The measurement of integrals in STARe software are done one by one and the integration limits are selected manually, so the measurement may not be accurate. But it can be said that the sum of the measured energies always returns a value corresponding to the energy exchanged for the complete transition.
To simplify the description, *Solid 1* (S1) is the solid phase that occurs during solidification and *Solid 2* (S2) is the phase formed after the solid-solid transition.
The behaviour of the S1-S2 transition peak is also analysed during heating. The curves reported in Figure 4-15 are obtained by heating the sample after it has been cooled to a speed of -650 K/s; phase S1 is freeze at room temperature and the solid-solid transition is avoided. The curves show that as the rate increase, the peak shift at higher temperatures. For heating rates higher than 1000 K/s there is even the overlap between the S1-S2 transition peak and the melting event.

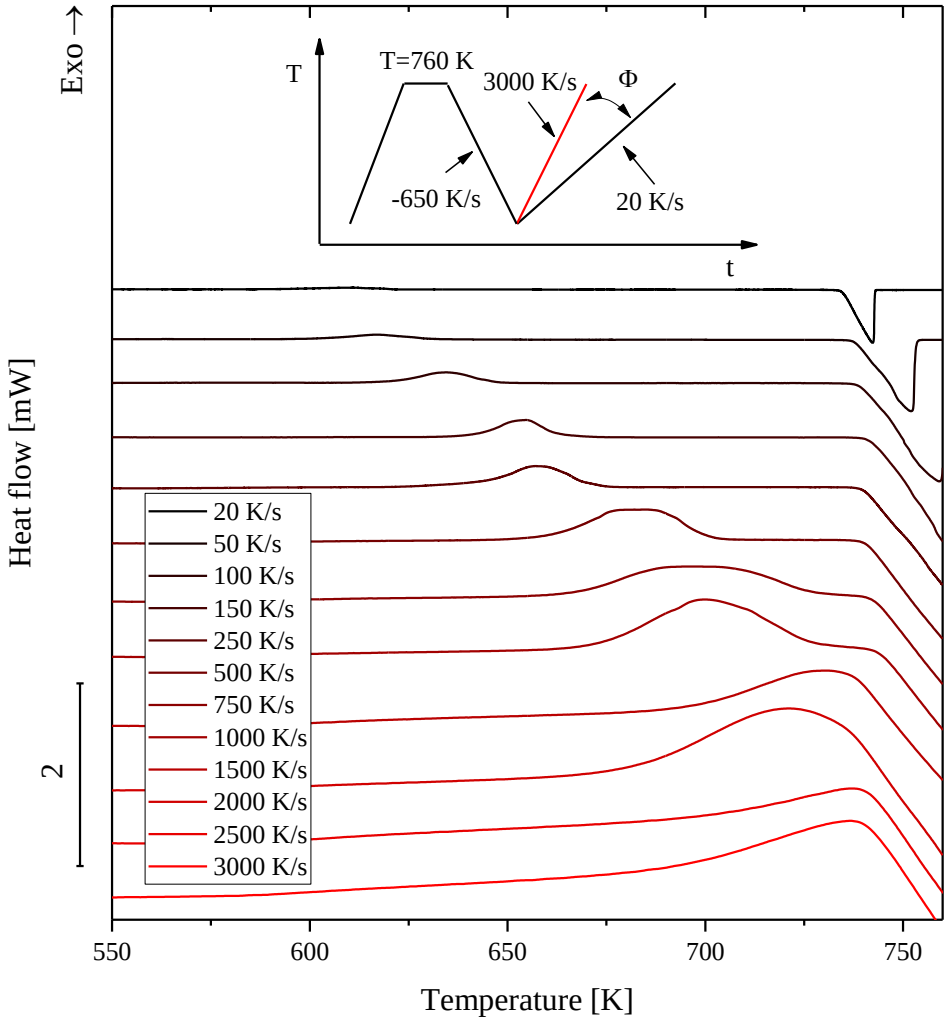

Figure 4-15 *FDSC curves obtained for heating rates between 20 and 3000 K/s after quenching.*

The shifting phenomenon of the peak for the solid-solid transition (S1-S2) is analysed using a Kissinger plot. It is based on measurements of the temperature at which the top of the peak is positioned.

The Kissinger plot obtained for S1-S2 transition is reported in Figure 4-16. This analysis is used to evaluate the activation energy of the concerned transition. The activation energy is calculated by multiplying the slope of the fitting line by the gas constant (R). The calculated activation energy for Al_3Mg_2 is E_a = 121.36 kJ/mol. The high value of R^2 means that the linear fit of the values represents very well the behaviour of the system.

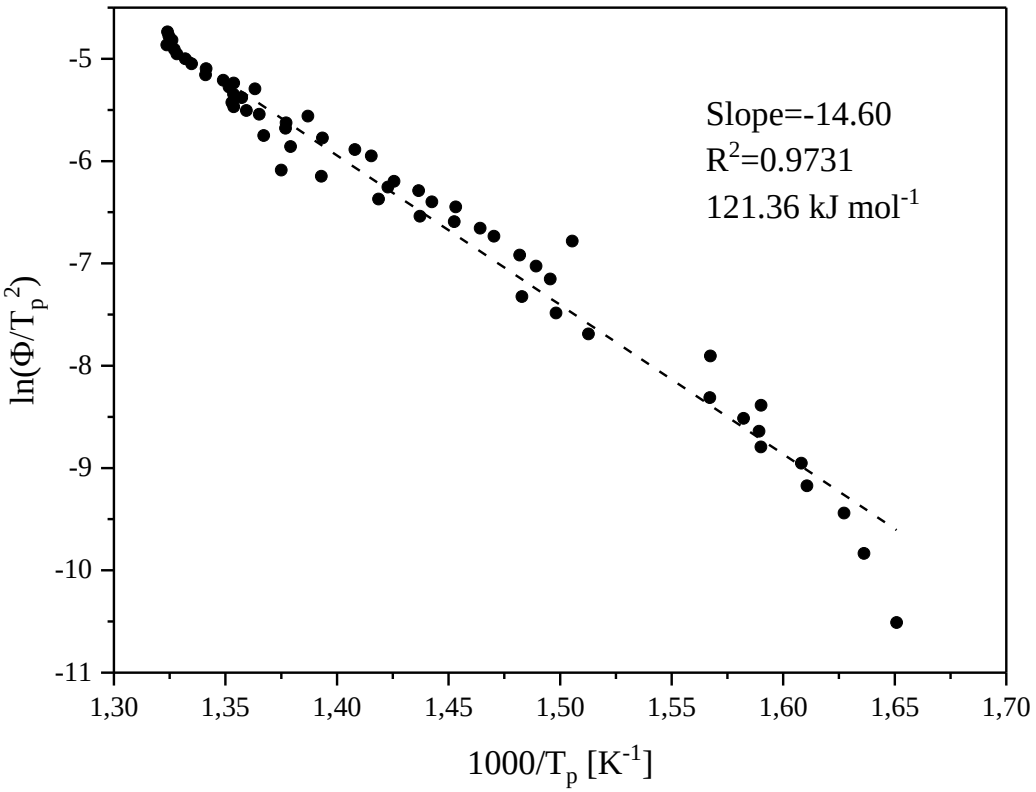

Figure 4-16 *Kissinger plot.*

In Figure 4-15 it is also possible to see that the melting does not happen always at the same temperature. It shifts at higher temperatures as the heating rate increase. A focus is made on this solid-liquid phase transition. The rate range between 10 and 1000 K/s is analysed; the results are shown in Figure 4-17. The fitting line has an R^2=0.981, this means that the model well represents the shifting of the melting T_{onset}. As the heating rate increase, the T_{onset} linearly increase with slope ($+9.53x10^{-2}$). The starting temperature after the temperature correction is T_m=734.60 K. This temperature does not correspond to the melting temperature previously evaluated, but this value could be attributed to an inaccurate

temperature correction. It can be assumed that the melting temperature at 10 K/s is ~725 K. The shift is attributed to the thermal lag of the instrument.

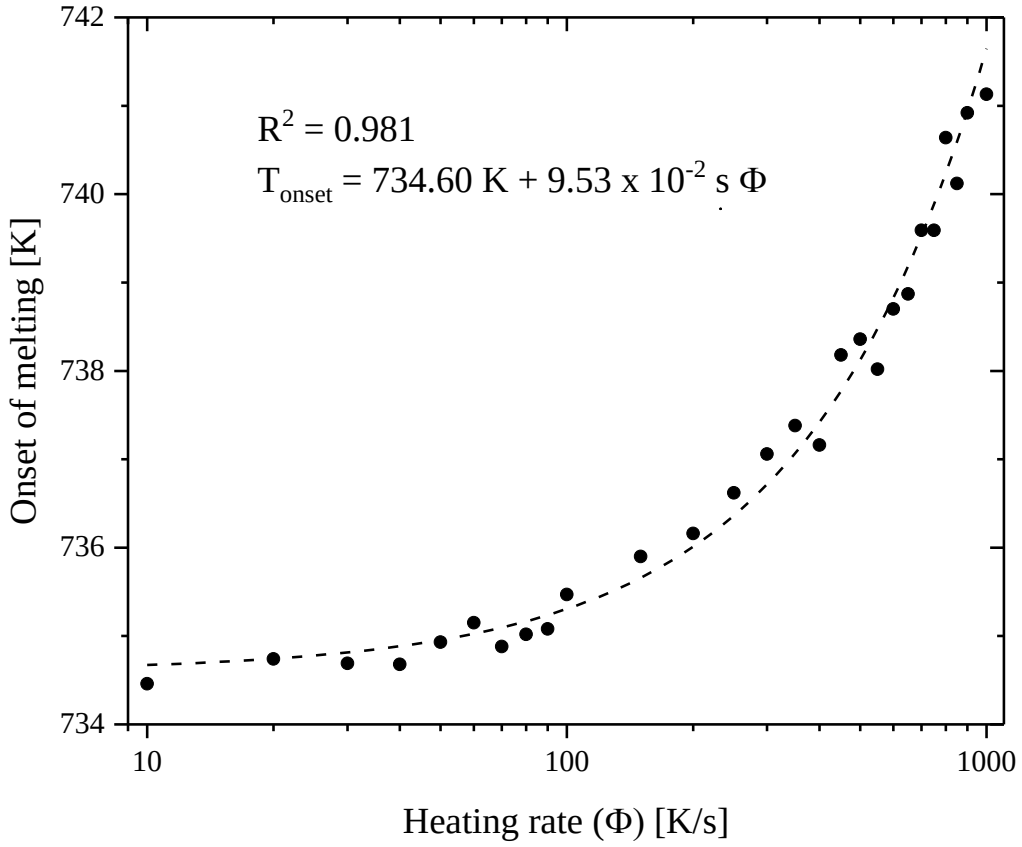

Figure 4-17 *Onset of melting.*

The solid-solid transition is also assessed under isothermal conditions. As it is shown in Figure 4-18, the S1 phase is frozen at room temperature applying a cooling rate of -650 K/s. Then, it is heated with the highest possible heating rate (10,000 K/s) up to the isothermal temperature. The applied isothermal temperature that are reported in the graph are between 623 and 673 K. In this way it is assumed that the transition does not have the possibility to start before it reaches the measurement temperature; therefore, the transition from S1 to S2 should return an exothermic peak in the curve described in the graph.

The curve at 623 K is almost flat; from the integral of the curve it is verified that all the energy expected for the transition is released, proving that the transition takes place completely. As the temperature at which the isothermal measurement takes place increases, the peak becomes increasingly narrow and high.

The time required to complete the transition is reduced from about 5 seconds to about 0.8 seconds increasing the isothermal segment in the temperature program from 623 to 673 K.

Lower temperatures are analysed but the low height of the peak did not allow neither to make adequate measurements of the heat exchanged, nor to see the presence or position of the peak.

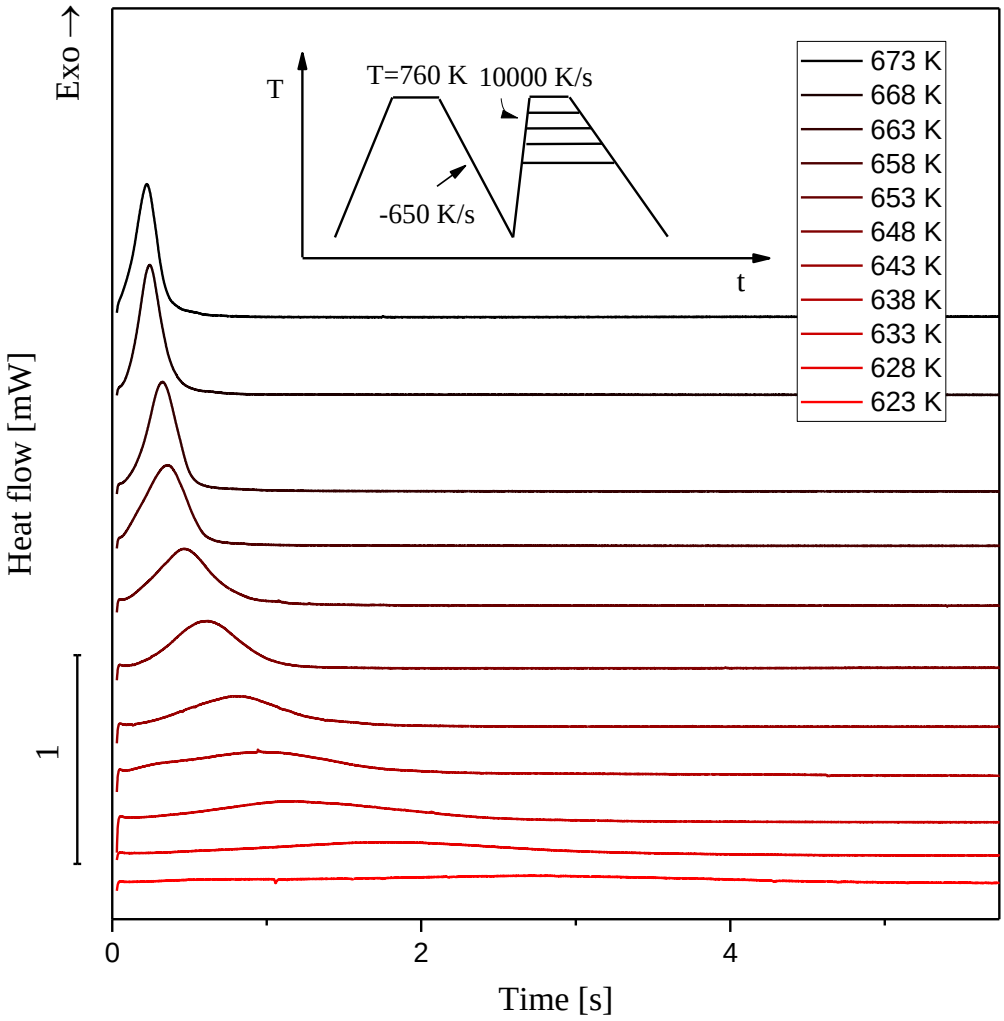

Figure 4-18 *Isothermal analysis of the solid-solid transition.*

About the S1-S2 transition peak it is possible to say that its shape is almost symmetric. A zoom on the transition peak obtained at the isothermal temperature 673 K is shown in Figure 4-19.

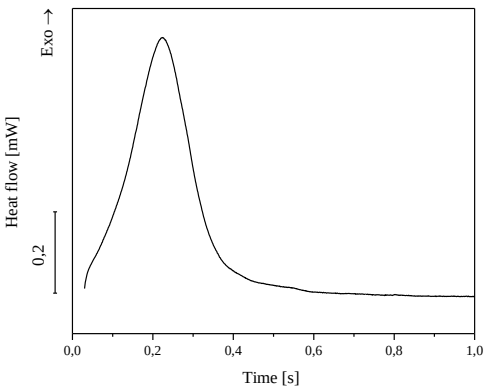

Figure 4-19 *Zoom on exothermic peak on S1-S2 transition obtained with isothermal analysis at 673 K.*

After this series of analyses, a Gibbs free energy diagram is supposed. The diagram (shown in Figure 4-20) is a schematic suggestion on the basis of obtained data, but it is not possible to define properly the position of the curves nearby the melting temperature. It is assumed that the curve of the *Solid 1* is always above the curve of the *Solid 2*, for $T<T_m$, because the phase transition S1-S2 always occurs before the melting of the intermetallic compound.

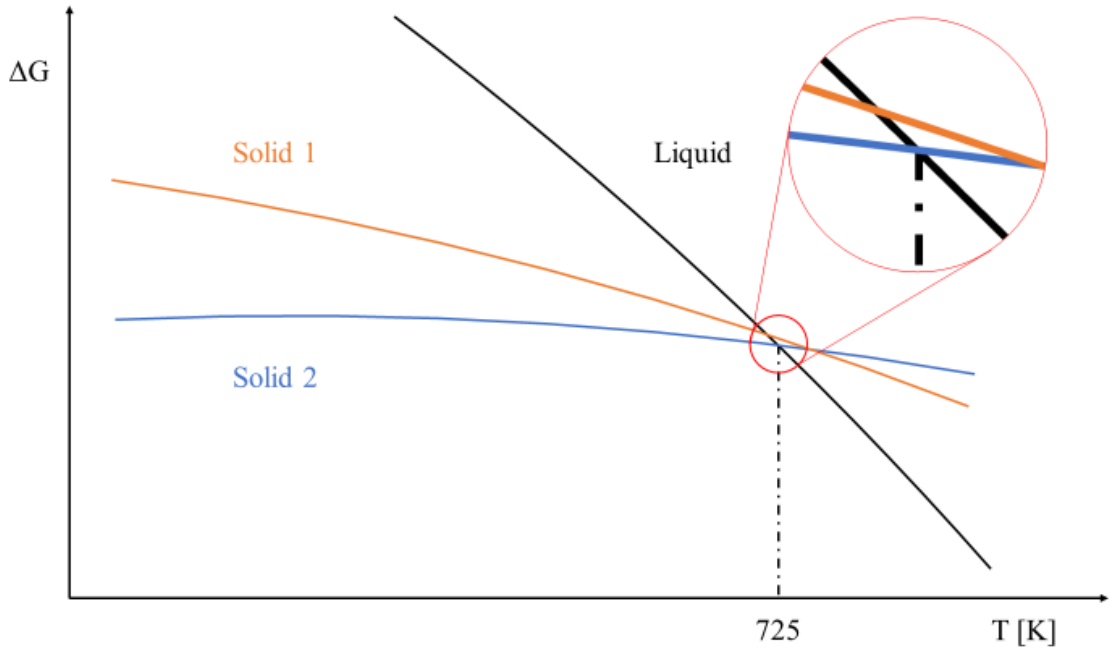

Figure 4-20 *Hypothesis of Gibbs free energy diagram.*

In addition, in order to clarify how this hypothesis is deduced, Figure 4-21 and Figure 4-22 show the analysed transitions and the respective paths upon cooling and heating. As already explained above, for cooling rates higher than -500 K/s, S1 is frozen at room temperature; instead, for cooling rates lower than -200 K/s the S1-S2 transition happen completely. In case of ranges in between there should be both S1 and S2 at room temperature.
Then, upon heating, the eventually present S1 would transform to S2 before the melting.

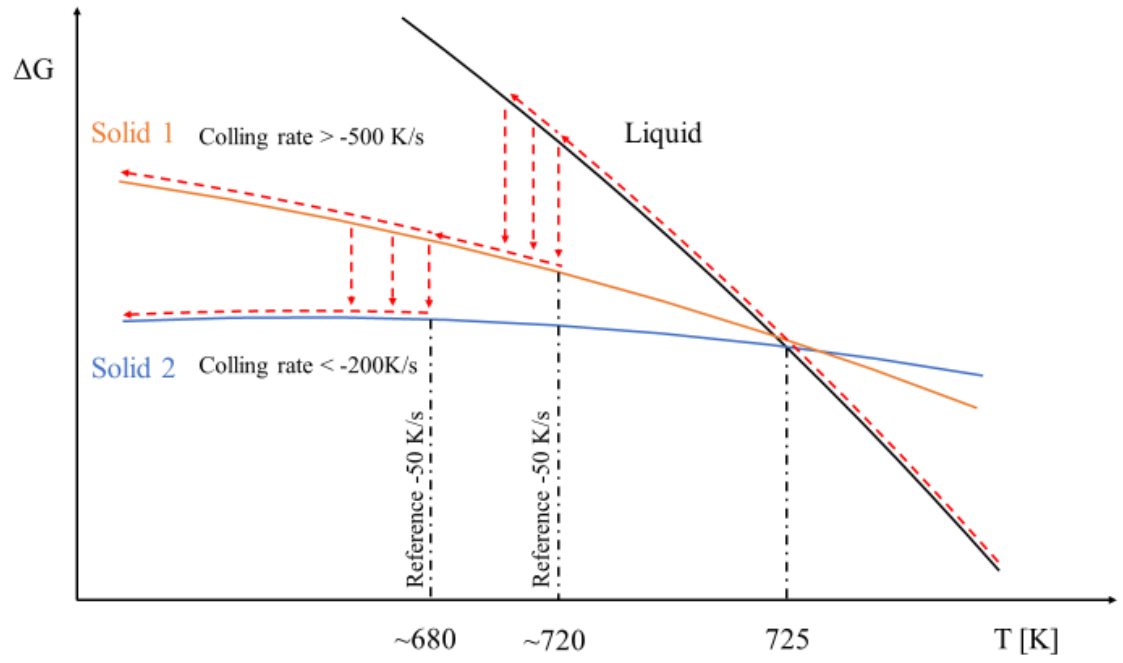

Figure 4-21 *Hypothesis of Gibbs free energy diagram. The red dashed line represents the path upon cooling.*

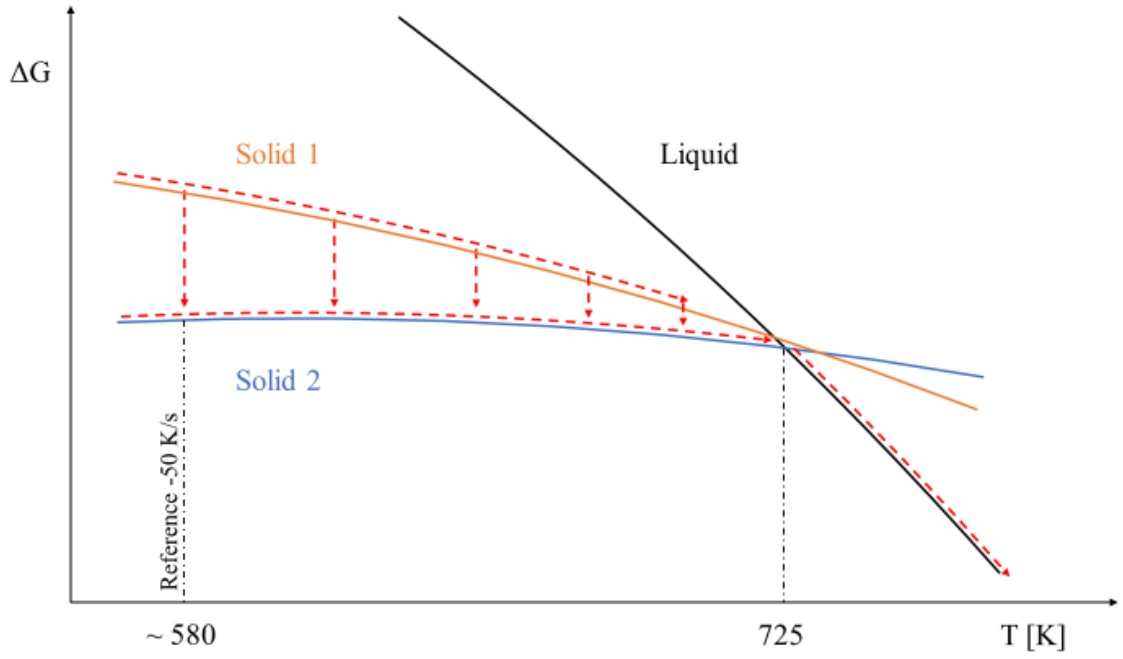

Figure 4-22 *Hypothesis of Gibbs free energy diagram. The red dashed line represents the path upon heating.*

5 Discussion

The study on Al_3Mg_2 demonstrated the presence of a phase transition that was not visible with a traditional DSC analysis. In particular, a solid-to-solid transition that was not expected by the Al-Mg phase diagram was identified. The phase transition was studied by applying various cooling and heating rates. It has been shown that *Solid 1*, which could be considered a metastable phase, can be stabilized at room temperature. The temperature range within which the transition partially occurs has been identified: from -200 to -500 K/s. In this case, at room temperature, both phases are present at the same time. Subsequently, during the heating stage, it is demonstrated that the transition from *Solid 1* to *Solid 2* always occurs completely before melting. A Kissinger plot has been performed and an activation energy for S1-S2 transition about E_a = 121.36 kJ/mol was evaluated.
Finally, isothermal analyses were carried out, always to evaluate the S1-S2 transition.
This analysis showed that the transition rate decreases as the temperature at which the isothermal stage is performed increases and that the transition peak has a Gaussian shape.
The phenomenon of solid-solid phase transition via melting, demonstrated by Pogatscher S. [1], was not identified in this study, even at high rates (1000 K/s).

6 Conclusion and Outlook

The purpose of this thesis was to apply the use of FDSC to an inorganic material with melting temperature within the temperature range of applicability of the sensor (up to 520 °C). Al_3Mg_2 has been identified as a candidate not only because his T_m falls within this range but also because the complexity of his unit cell made him more interesting for the purpose. The application of unconventional cooling rates (not achievable with DSC) had to show the possibility of leading to the formation of metastable or amorphous phases. Finally, it was of interest to verify whether the eventual solid transition was characterized by the formation of a liquid intermediate state as demonstrated by Prof. Pogatscher in a previous study on another alloy.

The first and difficult part of the thesis was dedicated to the preparation that required a great effort and a lot of time. The presence of unwanted compounds in the intermetallic compound required testing different configurations before obtaining a sample with the desired characteristics. The procedure has shown many critical points and in the case of subsequent tests it is advisable to use a vacuum furnace, which was not available at the time.

The results have shown that the use of FDSC allows to study in greater depth and with better resolution phase transitions. An unexpected solid-solid transition was identified and analysed; but the formation of a liquid intermediate phase during the solid-solid transition did not occur.

There are still some aspects to be clarified regarding this specific intermetallic compound. It might be interesting, in the case of subsequent studies, to perform TEM analysis for the determination of the crystalline structures of Solid 1 and Solid 2. This could help to better understand the nature of the two phases and the reason why this reaction is not identified in the phase diagram.

Acknowledgments

I would like to thank Prof. Stefan Pogatscher, who gave me the opportunity to do my thesis work at Montanuniversität Leoben and to get to know an innovative technology such as FDSC.

Thanks also to Cameron, who helped me with the experimental tests on Flash DSC1, and to the whole department that welcomed me with affection.

My greatest gratitude to Prof. Irene Callari, thanks to whom I was able to spend a wonderful experience in Austria for the development of the thesis.

A heartfelt thanks to my parents, my sister, my nephews, my brother-in-law and all the members of my family; they are always there for me and they are the backbone of my life.

Thanks also to my girlfriend Viola, with whom I spent beautiful days. Thank you for the experiences we have had together and for your constant support.

Finally, not by importance, a special thank you to my friends, roommates and colleagues from university who shared with me wonderful moments during university life.

References

[1] S. Pogatscher, D. Leutenegger, J.E.K. Schawe, P.J. Uggowitzer, J.F. Löffler, Solid-solid phase transitions via melting in metals, Nature communications 7 (2016) 11113.

[2] D.A. Porter, K.E. Easterling, M.Y. Sherif, Phase transformations in metals and alloys, CRC Press, Boca Raton, FL, 2009.

[3] W. Steurer, The Samson phase, β-Mg2Al3, revisited, Zeitschrift für Kristallographie 222 (2007) 2513.

[4] H. Okamoto, Al-Mg (aluminum-magnesium), JPE 19 (1998) 598.

[5] Sten Samson, The Crystal Structure of the Phase II MgzAI3, Acta Crystallographica 19 (1965) 401–413.

[6] J. Wolny, M. Duda, B. Kozakowski, Simple model of Mg 2 Al 3 β and β' phases, J. Phys.: Conf. Ser. 226 (2010) 12035.

[7] J. Wolny, B. Kozakowski, M. Duda, J. Kusz, Stacking of hexagonal layers in the structure of β-Mg 2 Al 3, Philosophical Magazine Letters 88 (2008) 501–507.

[8] C.D. Treviño-Quintanilla, R. Krishnamoorti, J. Bonilla-Ríos, Flash DSC crystallization study for blown film grade bimodal HDPE resins. I. Isothermal kinetics and its application of the blown film modeling, J. Polym. Sci. Part B: Polym. Phys. 54 (2016) 2425–2431.

[9] J.E.K. Schawe, Influence of processing conditions on polymer crystallization measured by fast scanning DSC, J Therm Anal Calorim 116 (2014) 1165–1173.

[10] S. Pogatscher, D. Leutenegger, A. Hagmann, P.J. Uggowitzer, J.F. Löffler, Characterization of bulk metallic glasses via fast differential scanning calorimetry, Thermochimica Acta 590 (2014) 84–90.

[11] Y. Corvis, A. Wurm, C. Schick, P. Espeau, Vitreous State Characterization of Pharmaceutical Compounds Degrading upon Melting by Using Fast Scanning Calorimetry, The journal of physical chemistry. B 119 (2015) 6848–6851.

[12] G. Kurtuldu, K.F. Shamlaye, J.F. Löffler, Metastable quasicrystal-induced nucleation in a bulk glass-forming liquid, Proceedings of the National Academy of Sciences of the United States of America 115 (2018) 6123–6128.

[13] R. Montanari, Tecniche sperimentali per la caratterizzazione dei materiali dal laboratorio alla produzione, Associazione italiana di metallurgia, Milano, 2005.

[14] P.J. Haines, Principles of thermal analysis and calorimetry, Royal Society of Chemistry, Cambridge, 2002.

[15] G. Höhne, W. Hemminger, H.-J. Flammersheim, Differential Scanning Calorimetry, 2nd ed., Springer Berlin, Berlin, 2010.

[16] Matthias Wagner, Thermal Analysis in Practice: Collected Applications, 2009.

[17] C. Schick, V. Mathot, Fast Scanning Calorimetry, Springer International Publishing; Imprint: Springer, Cham, 2016.

Websites and pictures references

https://www.nanoscience.com/

https://www.mee-inc.com/

https://www.labcompare.com/617-News/1006-Mettler-Toledo-Introduces-the-Flash-Differential-Scanning-Calorimeter-Flash-DSC-1/

https://www.micro-shop.zeiss.com/pimages/10211_lg.jpg

https://dcyd0ggl1hia3.cloudfront.net/fileadmin/_processed_/opt_DSC_204_F1_Phoenix_Principle_Heat_Flux_DSC_1_1bed272fb4.png?1439997830

https://encrypted-bn0.gstatic.com/images?q=tbn:ANd9GcSCqM2zCM0ktsGLY4lSXVWkmzhWh1LOb-wGK9wwYfPST80jOZiQ

https://www.researchgate.net/profile/Hrishikesh_Das2/publication/253690045/figure/download/fig17/AS:638889429590041@1529334518490/Principle-of-EDS-spectroscopy.png

https://www.researchgate.net/profile/Tanvir_Alam2/publication/254707658/figure/fig3/AS:314240767414274@1451932245636/Shows-the-basic-block-diagram-of-a-Scanning-Electron-Microscope.png

List of abbreviation

°C	Degree Celsius
A	Area
Å	Ångström
Al	Aluminium
Al_2O_3	Alumina
at.%	Atomic percentage
at. wt.	Atomic weight
C	Carbon
cm	Centimetre
DCS	Differential Scanning Calorimetry
d_e	External diameter
d_i	Inside diameter
DTA	Differential Thermal Analysis
EDS	Energy dispersive X-ray spectroscopy
Endo	Endothermic
Exo	Exothermic
FDSC	Flash Differential Scanning Calorimetry
g	Gram
h	Height
J	Joule
K	Kelvin
L	Length
mbar	Millibar
Mg	Magnesium
Mg_2Si	Magnesium silicide
mm	Millimetre
ms	Milliseconds
O	Oxygen
OM	Optical Microscope
R^2	Coefficient of determination
s	Second
S1	Solid 1
S2	Solid 2
SEM	Scanning Electron Microscope
Si	Silicon

T	Temperature
t	Time
T_{endset}	Endset temperature
T_g	Glass transition temperature
T_m	Melting temperature
T_{onset}	Onset temperature
T_r	Reference temperature
T_s	Sample temperature
V	Volume
wt	Weight
wt.%	Weight percentage
ΔT	Difference in temperature

List of tables

List of figures